JET-P(95)47

# Impurity Induced Neutralization of MeV Energy Protons in JET Plasmas

A A Korotkov[1], A Gondhalekar.

JET Joint Undertaking, Abingdon, Oxfordshire, OX14 3EA, UK.
[1] A F Ioffe Institute, St Petersburg, Russia.

Preprint of a paper submitted for publication in
Nuclear Fusion

Spetember 1995

## ABSTRACT

A neutral particle analyzer (NPA) was deployed on JET for measurement of distribution function of MeV energy protons driven by high power ion cyclotron resonance frequency heating of deuterium plasmas in the hydrogen minority scheme (D(H) ICRF heating). Unexpectedly, efficient neutralization of MeV energy protons was observed in the plasma center, without recourse to injection of a beam of atoms to provide charge donors for charge-exchange (CX) neutralization reactions. This paper presents a model elucidating the role of carbon and beryllium, the main impurities in JET plasmas, in this process and establishes charge exchange between hydrogen-like ([H]) ions of the impurities and protons as the main neutralization process. A model calculation for deducing the proton energy distribution function $f(E_P)$ from measured hydrogen flux is described. Uncertainties in cross-sections and their effect on the inferred $f(E_P)$ are examined. Validity of this model of Impurity Induced Neutralization (IIN)[1] is tested by using it to describe the measured hydrogen flux in different conditions of plasma heating and fueling. Using this model and a procedure in which a known change in density of deuterium atoms at the plasma center is made by applying neutral beam injection (NBI), we have deduced the background thermal deuterium atom density at the plasma center, which is an important new diagnostic result. Concerning future experiments, the model predicts that carbon and beryllium impurities will be major contributors to neutralization of hydrogenic ions in ITER, for ion energies $E_P \leq 1$MeV/u. According to these estimates measurement of ICRF driven hydrogenic ions in ITER plasmas will be possible without recourse to injection of atomic beams, using an NPA instrument similar to that used on JET.

# 1. EXPERIMENTAL SET-UP AND OBSERVATION OF "PASSIVE" AND "ACTIVE" HYDROGEN FLUX DURING D(H) HEATING

The NPA is of the conventional E || B type with eight energy channels having common mass selection, capable of time resolved measurements of H, D, T, He-3 and He-4 atomic flux emitted by the plasma, in the energy range $0.3 \leq E(MeV) \leq 3.5$ [2]. The experimental set-up is shown in fig.1. The NPA beam line geometry determined that only atoms with $v_Z/v_\phi \geq 2x10^2$ entered the NPA, where $v_Z$ is velocity towards the NPA and $v_\phi$ is that perpendicular to the line-of-sight. The area viewed by the NPA on the torus mid-plane was 5cmx5cm and the collecting solid-angle was $1.3x10^{-6}$ sterad. The vertical extent of the volume from which the observed flux originated, $2\Delta Z$, was determined by the vertical extent of the ICRF power deposition region, usually $\Delta Z = \pm 0.3$m as determined by ray-tracing calculations of ICRF power deposition. Thus the observed hydrogen flux arose from neutralization of energetic protons having their banana tips in the ICRF resonance layer and on the NPA line-of-sight.

In a typical experiment[3], pulse #27368, a deuterium plasma with $I_\phi = 3.5$MA and $B_\phi = 2.9$T was heated, at the time of the measurements to be discussed subsequently, by $\cong$ 5MW of ICRF power at 42.6MHz for D(H) heating, $\cong$ 1.6MW of 130kV deuterium NBI from oct.8, and $\cong$6 MW of 120kV helium-4 NBI from oct.4. The neutral beam at each octant consisted of two banks, "normal" and "tangential". Each bank consisted of four sub-beams (PINI sources) arranged vertically, as in fig.1. The NPA line-of-sight passed in the middle between the "tangential" and "normal" bank beams. The NPA line-of-sight intersected the ICRF heating profile which peaked near the major radius of the plasma column. Fig.2 shows evolution of plasma parameters and hydrogen flux received into the NPA. Notice that the high energy hydrogen flux to the NPA arose soon after ICRF power was applied and independently of the oct.4 NBI. We call this the "passive" flux. The data shown here, incorporating new calibration of the NPA subsequent to [3] differs from that shown in reference[3] and supersedes it.

Fig.3 shows calculated orbit of a 0.5MeV proton with $v_Z/v_\phi = 2x10^2$ in pulse #27368 at 6.4s, the tip of its banana orbit was specified to be on the NPA line-of-sight and within the ICRF power deposition region. Such calculations were repeated for energies spanning the range of measurement in these experiments, $0.3 \leq E(MeV) \leq 1$. These orbits show that in analyzing the measured hydrogen flux arising from neutralization of ICRF driven MeV energy protons in JET only the central region of the plasma need be considered.

Before these experiments were performed the expectation was that a measurable flux of hydrogen would arise only with application of NBI from oct.4 due to direct CX between protons and beam atoms. Therefore the "passive" flux seen in fig.2 was not expected. The

"active" flux, arising only when oct.4 NBI and ICRF were applied together, is also seen in fig.2. However in other pulses with D(H) ICRF heating a flux of high energy hydrogen, approximately equal to the "active" flux, was observed when NBI was applied only at oct.8, as shown in fig.14. This latter observation suggests that the "active" flux is not related entirely to direct CX of protons with NBI atoms at oct.4. In fig.4 the energy distribution of the hydrogen flux, $\Gamma(E_H)$, is shown for two time points in the pulse, at 6.4s (curve #1) and 6.6s (curve #2), for the "passive" and "active" fluxes respectively.

Comparing curves #1 and #2 in fig.4, the uniform increase in the "active" flux by a factor of $\cong$3.5 over the "passive" one and the observation of fig.14 mentioned above suggest that injection of atoms into the plasma using NBI amplifies the process giving rise to the "passive" flux, which we postulate to be charge-exchange between [H] impurity ions and protons. We attribute the difference in $\Gamma(E_H)$ between the "active" and "passive" fluxes at energy $E_H$(MeV)<0.5 to direct CX of protons with the helium atoms injected at oct.4.

## 2. NEUTRALIZATION MECHANISMS FOR MeV ENERGY PROTONS

Before these measurements in JET it was thought that two well known processes, CX between protons and atoms and radiative recombination of protons and electrons, would account fully for the neutralization.

### 2.1 Charge-exchange between protons and NBI atoms

First CX between protons and injected atoms, which was expected to be the dominant neutralization process for protons, is represented by

$$p + A \rightarrow H^0 + A^+ \qquad \text{eq.1}$$

Here p, A, $H^0$ denote protons, electron-donors and hydrogen atoms. Cross-sections for the reaction have been measured with 20-40% accuracy in the range $E_P$<7.5 MeV for atomic hydrogen as donor, and with accuracy of 20% for $E_P$<11 MeV for atomic helium as donor[4].

Fig.4(curve #4) shows the expected $\Gamma(E_H)$ if only the above process, in conjunction with oct.4 NBI, were contributing to proton neutralization in the "active" flux. Lastly (a) CX of protons with thermal deuterium atoms, present in the plasma due to recycling at the plasma boundary, must be taken into account; however the density of such atoms is usually very low and their contribution negligible, (b) significant neutralization of protons by halo atoms, produced when atomic beams are injected into plasmas, is also possible; but this effect is

important only in high density plasmas with $n_e > 6x10^{19}$ $m^{-3}$. These two points will be addressed again later.

## 2.2 Radiative recombination with thermal plasma electrons and with "cold" electrons from neutral beam injection

Second, radiative recombination of protons and electrons is given by

$$p + e \rightarrow H^0 + \text{photon} \qquad \text{eq.2}$$

Exact quantum mechanic analytic expressions for cross-sections for this process in the non-relativistic Born approximation exist[5]. The corresponding rate coefficient is proportional to $T_e^{-3/2}$ for values of plasma electron temperatures $T_e$ relevant here and happens to be small. Fig.4(curve #3) shows expected $\Gamma(E_H)$ if recombination were the only proton neutralization process operating in giving the "passive" flux.

With respect to the "active" flux, the recombination efficiency could be increased in the measurement volume due to "cold" electrons born from ionization of NBI atoms. These electrons have an initial directed velocity equal to that of NBI atoms and the corresponding electron energy, for beams used in JET experiments, would be 16-35 eV. The thermalization time for such electrons in typical JET plasmas is $\tau_T \leq 2x10^{-4}$ s.

The ratio $\beta_r$ of rate coefficients for recombination with "cold" electrons and that with "hot" plasma electrons is given by,

$$\beta_r = [\, T_e / T_{e(cold)} \,]^{3/2} \, . \, n_{e(cold)} / n_e \qquad \text{eq.3}$$

$T_{e(cold)}$ and $n_{e(cold)}$ are effective temperature and density of "cold" electrons whereas $T_e$ and $n_e$ are for plasma electrons. The equilibrium density of the "cold" electron population, $n_{e(cold)}$, can be estimated as

$$n_{e(cold)} = I_b \, . \, n_b \, . \, n_e \, . \, \tau_T \, . \, \Delta L_b / 2\pi R \qquad \text{eq.4}$$

$I_b$ is the ionization rate coefficient for beam atoms, $n_b$ is beam atom density at the plasma center and $\Delta L_b$ is the toroidal extent of the beam. In a time interval much shorter than $\tau_T$ the "cold" electrons spread around the torus, the term $\Delta L_b/2\pi R$ in eq.4 takes into account the consequent averaging of $n_{e(cold)}$.

Since the velocity of the observed protons is larger than that of "cold" electrons we assume that $T_{e(cold)} = [m/M] . E_p$ where m/M is the ratio of electron to proton masses. We then have

$$\beta_T \approx 10^5 . (T_e/E_P)^{3/2} . I_b . n_b . \tau_T . \Delta L_b/2\pi R \qquad \text{eq..5}$$

Since $(I_b . n_b) < 25 s^{-1}$ in JET plasmas, we obtain for the lowest energy protons measured, 0.3MeV, that $\beta_T < 2x10^{-2}$. Thus, because of rapid thermalization of "cold" electrons, their contribution to radiative recombination is much less than that of plasma electrons.

We therefore conclude that the two processes discussed above, direct CX with beam atoms and radiative recombination either with plasma electrons or "cold" beam electrons, are not sufficient to give either the observed large hydrogen flux or its energy dependence. We shall show that the dominant neutralization process for fast protons in JET plasmas is CX between protons and [H] ions of impurities. We shall illustrate this with an experimental example in which the main plasma impurities were C, Be and He. The CX reactions in question are

$$p + A^{(Z-1)+} \rightarrow H^0 + A^{Z+} \qquad \text{eq.6}$$

Here $A^{(Z-1)+}$ stands for [H] ion of impurity with nuclear charge Z. We shall call the process in eq.6 Impurity Induced Neutralization (IIN). Two key circumstances determine that IIN plays a dominant role in JET plasmas, they are

1. [H] impurity ions $C^{5+}$, $Be^{3+}$ and $He^{1+}$ have the largest cross-sections for CX with protons in the energy range under consideration.
2. A high density of [H] ions of C and Be is normally found in JET plasmas, comparable with that of NBI atoms at the plasma center.

## 3. CROSS-SECTIONS FOR CX BETWEEN PROTONS AND [H] AND [He] IONS OF CARBON, BERYLLIUM AND HELIUM

It should be emphasized that CX only from ground state of the ions is important for these considerations because of very low population of excited ionic states in typical tokamak plasmas. Population of excited states of [H] ions has been calculated using the MIXSTN code[35]. For plasmas with $1 \leq T_e(keV) \leq 10$ the maximum population of the most populated state with principal quantum number n=2 (including metastable states) compared with that of the n=1 ground state can be estimated as $\cong 2x10^{-5}$, independent of $n_e$ and ion nuclear charge Z, for $Z \geq 4$. This is because the 2s and 2p states are not mixed for such ions due to

comparatively large Lamb shift and fine splitting. On the other hand the population of $He^+(n=2)$ state depends linearly on $n_e$ but does not exceed $1x10^{-4}$ for $n_e \leq 10^{20}$ $m^{-3}$.

We note that the relative translational energies of ions in the CX reactions of interest here are $0.1 \leq E(MeV/u) \leq 3$, which corresponds to a velocity interval $2 < v(a.u.) < 11$. Since the orbital electron velocity $v_0$ in the ground state of [H] ions is equal to Z(a.u.) we see that the energy interval under study is very wide and includes the adiabatic range ($v \ll Z$) for $Be^{3+}$ and $C^{5+}$ as well as the Born range ($v \gg Z$).

The total CX cross-section has been measured for $E_P < 200$ keV only for the reaction

$$p + He^+ \rightarrow H^0 + He^{2+}$$

Since measurements of the required cross-sections are not available, in this report we shall use computed values based on the best founded theoretical calculations. In the following we briefly characterize these calculations and estimate the accuracy of cross-sections thus obtained.

### 3.1 (p + [H]-ion) CX reactions in the low energy range, v « Z

For $v \ll Z$ we use the adiabatic theory based on analytic properties of molecular state energy function in the complex plane of internuclear distance R, Asymptotic Theory of Non-adiabatic Transitions(ATNT)[6]. Because of localization of electron transitions in R-space in the adiabatic range it is possible to take into account all interacting states at given value of *Re*R. It is important that the number of such states is much smaller than that for all values of *Re*R, it allows successive inclusion of extremely large number of interacting states, far exceeding the capability of the strong coupling calculations. The latter is especially important for the strongly asymmetric systems considered here in which a lot of intermediate states bridge the large energy gap between the initial $1s\sigma$ - state and the state correlating with 1s hydrogen state.

Because all interacting states appear in ATNT as different branches of sheets of the same analytic molecular state energy function there is no need for state basis choice, thereby avoiding difficulties in the strong coupling approach.

The calculations[7] used here take into consideration ≅200 interacting molecular states, allowing computation of CX cross-sections for transitions into hydrogenic states with n=1,2,3,4 for reaction ($p + He^+$), with n = 1,2 for reaction ($p + Be^{3+}$), and with n = 1 for the ($p + C^{5+}$) reaction. Contribution of transitions into excited states for the ($p + He^+$) and the

($p + Be^{3+}$) reactions is <5% in the adiabatic range and ≅20% in the vicinity of the cross-section maximum. The latter characterizes the possible underestimation of the cross-section for the ($p + C^{5+}$) reaction in the calculation.

For $v < Z/10$ one can expect good accuracy for the ATNT calculation, of order v/Z. At higher velocities the adiabatic conditions are violated for the "high" transitions, although the major transition $1s\sigma \rightarrow 2p\sigma$ is properly described beyond the cross-section maximum up to $v \approx Z\sqrt{Z}$. From a comparison of calculations for the ($p + He^{+}$) reaction with measurements [8,9,10] and other calculations [11,12,13] we conclude that an accuracy of ≈ 30-40% can be achieved even in the vicinity of the cross-section maximum, as shown in fig.5.

### 3.2 (p + [H]-ion) CX reactions near the cross-section maximum, $v \cong Z/\sqrt{2}$

In the vicinity of the cross-section maximum ($v \cong Z/\sqrt{2}$) we use results of total cross-section calculations using the Coupled Sturmian Pseudo-state Approach(CSPA)[11]. The accuracy of the cross-sections is 10-20% for $0.2 \leq v/Z \leq 1$, estimated from convergence of results with increase of state basis size. An advantage of the Sturmian basis is that states with positive energy exist. This allows a better description of electron transitions through intermediate states not bound to either nucleus, and extension of the calculations up to the high velocity range where perturbative models become valid. An example is a calculation[14] for the ($p + He^{+}$) reaction, fig.6. The calculation describes well the measurements near the cross-section maximum and accords with the DSPB calculations below with 30% accuracy up to an energy of 0.8 MeV/u.

### 3.3 (p + [H]-ion) CX reactions in the high energy range, v > Z

In the high energy range (v>Z) we make use of results of calculations employing the first-order Continuum Distorted Wave approximation(CDW1) [15] for CX into 1s and 2s states. This is a consistent approach in the frame of well known Distorted Wave(DW) methods [16].

For comparison we present also results of two other calculations based on the DW method, the Boundary Corrected First Born approximation(B1B) [17] and Channel Distorted Strong Potential Born approximation(DSPB) [18]. DSPB is a method of higher order than CDW1 and B1B because both discrete and continuum levels are represented by exact wave functions of the electron in the field of the strong potential. On the other hand the weak potential is represented in lowest order. Thus better accuracy is expected of the method for highly asymmetric systems.

We have estimated cross-sections for CX into the ground state using the DSPB approach for the $(p + Be^{3+})$ and $(p + C^{5+})$ reactions. For this purpose we use the universal cross-section from impulse approximation [19] and the $|M|^2$-factor, taking into account elastic scattering and off-energy-shell effects in the DSPB method [18].

Results shown in fig.7 and fig.8 demonstrate convergence of all calculations at high energies. As expected the DSPB calculations agree better with CDW and B1B calculations for the more asymmetric $(p + C^{5+})$ system. CDW calculations [15] for the $(p + He^{+})$ system, fig.6, seem to underestimate the cross-sections. In this case we use results of CSPA and DSPB calculations from [14].

For analysis of the accuracy of cross-sections considered here it is necessary that convergence of perturbative methods based on the DW approach has been reliably established. Contribution of second order in the Boundary Corrected Born approach for the (p+H) system has been shown to be about 30% at v = 2.2 a.u.[20], which is close to that for $1s \rightarrow 1s$ transition in the simplified CDW approach(TCDW)[21], $\cong 1/v^2$ . We expect the largest second order corrections in CDW itself to be at $v \gg Z$ because of Thomas double scattering. According to [22] corrections of order $(Zn)^{-1}$, where $Z \gg 1$ and n is the principal quantum number of the final state, apply to transitions into excited states of the projectile. Therefore the total cross-section in CDW2 should be very close to that in CDW1 calculations.

From the above analysis we can draw the following conclusions about the accuracy of the cross-sections to be used in what follows,

a. in the adiabatic range ($v \ll Z$) we have good accuracy, of order $\approx v/Z$,
b. in the vicinity of the cross-section maximum the accuracy of calculations is 20-30% for the $(p + Be^{3+})$ and $(p + C^{5+})$ systems, whereas the accuracy of the measured cross-sections for the $(p + He^{+})$ system is about 10%,
c. beyond the cross-section maximum the accuracy is determined by contribution of CX into excited states and contributions of second order in the CDW approach. Contribution of CX into the 2s-state in the calculation [15] is $\cong 10\%$, which is in accordance with asymptotic behaviour like $n^{-3}$. So the total accuracy can be estimated as 20%. Notice that this conclusion is confirmed by comparisons of results of different calculations at high energies in fig.6, fig.7 and fig.8.

### 3.4 (p + [He]-ion) CX reactions

For the (p + [He]-ion) reactions we use CX cross-sections calculated using the two-orthogonal state expansion method[23].

Lastly, fig.9 summarizes cross-sections compiled from calculations and measurements discussed in this section. These cross-sections will be used in subsequent analysis of hydrogen fluxes from the plasma. We see that for $E_P \geq 0.5$MeV cross-sections for CX with [H] ions of C and Be impurity are larger than those for CX with deuterium and helium atoms.

## 4. MODELLING OF PROTON NEUTRALIZATION AND INFERENCE OF ENERGY DISTRIBUTION FUNCTION $f(E_P)$

Following section 2 an expression for total proton neutralization probability can be written as

$$P_V(E_i) = n_b\langle\sigma v\rangle_{CXb} + n_d\langle\sigma v\rangle_{CXd} + n_h\langle\sigma v\rangle_{CXh} + \sum_q n_q\langle\sigma v\rangle_{CXq} + n_e\langle\sigma v\rangle_r \qquad \text{eq.7}$$

$\langle\sigma v\rangle_{CXb,d,h,q}$ are respectively rate coefficients for CX of protons with beam atoms, thermal deuterium atoms, halo atoms and impurity ions, and $\langle\sigma v\rangle_r$ is the radiative recombination rate coefficient. $n_{e,b,d,h,q}$ are densities of electrons, beam atoms, thermal deuterium and halo atoms, and [H] and [He] ions of impurities under consideration.

$\bar{f}(E_i)$, the proton energy distribution function at energy $E_i$ in the NPA solid angle integrated along the NPA line-of-sight, is inferred from the relation

$$\bar{f}(E_i) \cdot P_V(E_i) \cdot \gamma(E_i) \cdot S \cdot \Delta E_i \cdot \mu_i = N_i \qquad \text{eq.8}$$

Index i is the NPA channel number with i=1,..8, $\gamma(E_i)$ is plasma transparency for hydrogen atoms seen in the channel, S is area viewed by the NPA in the observation volume at the plasma mid-plane, $.\Delta E_i$ is energy width of each channel, $\mu_i$ is detection efficiency for each channel, and $N_i$ is measured count rate of hydrogen atoms in the NPA after subtracting background noise count rate due mostly to neutrons, The neutron background count rate in a channel is determined using measured total neutron production rate and a separate measurement of neutron detection efficiency for each channel.

Fig.10 shows schematically how different computations are linked in modeling the measured hydrogen flux. The required CX cross-section data is drawn from an atomic data base, plasma pulse parameters such as $n_e$, $T_e$, $T_i$, $Z_{eff}$, bare ion densities for impurities $He^{2+}$, $Be^{4+}$, and $C^{6+}$, NBI and ICRF heating details from the processed data files, and NPA details such as S, $E_i$, $\Delta E_i$, $\mu(E_i)$, and $N_i$ from other data files. The codes first calculate densities $n_b$ and $n_h$ of neutral deuterium in the plasma core due to NBI and its halo. A value for $n_d$ the density of thermal deuterium atoms due to recycling is assumed. The codes next compute, using measured impurity nuclear densities and an impurity ionization balance model, densities $n_q$ of [H] and [He] ions of the impurities. From the above the codes compute the total proton neutralization probability $P_V(E_i)$. Seperately the codes compute $\gamma(E_i)$ the plasma transparency for exiting hydrogen atoms which, together with the measured hydrogen flux at the NPA, yields the hydrogen flux at the source. The proton energy distribution function $\bar{f}(E_P)$ is then deduced as shown in eq.8.

### 4.1 Calculation of donor densities in the plasma core

In this section we describe the model developed for calculation of $n_q$, the density of the donors in eq.7, where $n_q$ includes [H] ions ($n_{Z-1}$) and [He] ions ($n_{Z-2}$) of C, Be and He. As described in section 1 most of the observed high energy hydrogen flux arises from the plasma core region and therefore we need consider only this region of the plasma for donor density calculations. We shall assume the core plasma to be uniform and stationary.

**1. Impurity ionization balance.**

We calculate impurity donor densities using a system of steady-state ion balance equations for bare, [H] and [He] ions of the impurities,

$$I_{Z-1}\, n_{Z-1}\, n_e = n_Z \Big\{ 1/\tau_Z + \alpha_Z\, n_e + \beta_Z\, n_d + (n_b \gamma_b \langle \sigma v \rangle^{b}_{CXZ} + \beta_Z\, n_h\, \gamma_h)_{oct.4} + (n_b \gamma_b \langle \sigma v \rangle^{b}_{CXZ} + \beta_Z\, n_h\, \gamma_h)_{oct.8} \Big\} \qquad \text{eq.9}$$

$$\begin{aligned} I_{Z-2}\, n_{Z-2}\, n_e = {} & n_{Z-1} \Big\{ I_{Z-1}\, n_e + 1/\tau_{Z-1} + \alpha_{Z-1}\, n_e + \beta_{Z-1}\, n_d + (n_b \gamma_b \langle \sigma v \rangle^{b}_{CXZ-1} + \beta_{Z-1}\, n_h\, \gamma_h)_{oct.4} \\ & + (n_b \gamma_b \langle \sigma v \rangle^{b}_{CXZ-1} + \beta_{Z-1}\, n_h\, \gamma_h)_{oct.8} \Big\} \\ & - n_Z \Big\{ \alpha_Z\, n_e + \beta_Z\, n_d + (n_b \gamma_b \langle \sigma v \rangle^{b}_{CXZ} + \beta_Z\, n_h\, \gamma_h)_{oct.4} \\ & + (n_b \gamma_b \langle \sigma v \rangle^{b}_{CXZ} + \beta_Z\, n_h\, \gamma_h)_{oct.8} \Big\} \end{aligned} \qquad \text{eq.10}$$

Eq.9 and eq.10 include rate coefficients for all important atomic process, $I_{Z-1, Z-2}$ for ionization of [H] and [He] impurity ions by electrons, $\alpha_Z$ for radiative recombination of bare impurity ions, $\alpha_{Z-1}$ for radiative and dielectronic recombination of [H] impurity ions, $\beta_{Z, Z-1}$ for CX of bare and [H] impurity ions with thermal deuterium atoms, and $< \sigma v >^{b}_{CXZ}$ and $< \sigma v >^{b}_{CXZ-1}$ respectively for CX of bare and [H] impurity ions with beam atoms.

Recall that the NPA is located at oct.4 and measures neutralization of protons at the center of plasma at that location. However, eq.9 and eq.10 contain contributions from beam and halo atoms due to atomic beams in both oct.4 and oct.8. This is because there is a possibility for [H] and [He] impurity ions from oct.8 to travel halfway around the torus to oct.4 without ionization and contribute to neutralization of protons in oct.4. Coupling of ionization balance between oct.4 and oct.8 during NBI is described in eq.9 and eq.10 by factors $\gamma_{b,h}$ where

$$(\gamma_{b,h})_{oct.4} = \left\{ 1 - \exp[ - \Delta l_{b,h} / v_T \cdot \tau_i ] \right\} / \left\{ 1 - \exp[ -2\pi R / v_T \cdot \tau_i ] \right\} \qquad \text{eq.11}$$

$$(\gamma_{b,h})_{oct.8} = \exp[ -\pi R / v_T \cdot \tau_i ] \cdot (\gamma_{b,h})_{oct.4} \qquad \text{eq.12}$$

$\Delta l_{b,h}$ is the beam/halo dimension in the toroidal direction, $v_T$ is the average thermal velocity of the impurity ions, $\tau_i$ is the impurity ionization time and R the torus major radius. $\gamma_{b,h}$ describes coupling of beam and halo contributions respectively to the ionization balance.

When $\tau_i \ll \Delta l_{b,h} / v_T \ll \pi R / v_T$ then [H] impurity ions created in oct.4 are unable to escape from the source region, giving $(\gamma_{b,h})_{oct.4} = 1$, and also ions created in oct.8 cannot reach oct.4, giving $(\gamma_{b,h})_{oct.8} = 0$. In the opposite case when $\tau_i \gg \pi R / v_T$ corresponding to full octant coupling, we obtain geometric factors $\gamma_{b,h} = \Delta l_{b,h} / 2\pi R$ and then the location of NBI becomes unimportant for producing that part of the "active" flux arising from impurity induced neutralization(IIN).

All rate coefficients in the system of eq.9 and eq.10 are known to an accuracy of 10-20% because of simplicity of atomic systems considered. The one exception is a part of coefficient $\alpha_{Z-1}$ in eq.10, that due to dielectronic recombination rate coefficient for [H] ions. To estimate this we use the Burgess formula [24]. Because ionization from excited states is not included in the rate coefficient our calculation over-estimates the [He] impurity ion density. Radial ion transport in eq.9 and eq.10 is described by an empirical confinement time $\tau_Z = n_Z / \text{div}\, \Gamma_Z$.

Parameters $\tau_Z$ and $n_d$, the impurity ion confinement time and thermal deuterium density at the plasma center, are usually not known. Nevertheless calculation of donor densities using eq.9

and eq.10 is possible in the following circumstances where either one or both can be neglected,

a. When only one impurity donor is dominant we need not consider $\tau_Z$ and $n_d$ separately but a joint parameter $\Lambda = 1/\tau_Z + \beta_Z . n_d$ .

b. When $n_b$, the NBI atom density, is so large that terms with $\tau_Z$ and $n_d$ become negligible.

c. In an NBI free plasma when either CX with background atoms dominates ion transport or when ion transport dominates, because then only one free iterative parameter is left.

The above possibilities for inference of unknown parameters in special cases are discussed further in section 4.2. Notice that a steady-state ion balance is calculated and therefore the modeling describes plasma processes with time scales much longer than characteristic impurity ionization time $\tau_i \leq$ 1msec.

We solve the system of eq.9 and eq.10 using nuclear impurity ion densities $n_Z$ at the plasma center measured using CX-spectroscopy [25]. Fig.11 shows the calculated time behaviour of density of [H] and [He] ions of C and Be impurities for pulse #27368 shown in fig.3. In fig.11 we see that the ratio of [H] to [He] carbon ion density $n_{C5+}/n_{C4+} \cong 10$ in the plasma without NBI. With ≅1.6MW deuterium NBI at oct.8 $n_{C5+}/n_{C4+}$ increases to ≅20. In the low density plasmas considered here NBI in oct.8 produces an increase in [H] C and Be ions in oct.4 comparable to that due to NBI in oct.4 directly, i.e. oct.8 and oct.4 are closely coupled due to low plasma density. When a further 6 MW of helium NBI is applied at oct.4 the ratio of density of [H] and [He] C and Be ions increases to ≅100. Note that the distribution of beam density in the vertical direction is not taken into account in fig.11 or in modeling the measured hydrogen flux because in the experiment we deduce $\bar{f}(E_P)$ which is integrated along the NPA line-of-sight. The data in fig.11 was computed under the assumption that the vertical extent of the neutral beams corresponds to that of one PINI source.

**2. Attenuation of NBI atoms and of exiting MeV energy hydrogen atoms:**

A calculation of attenuation of the injected atomic beams is required in order to obtain the density of atoms in the interaction volume, and a calculation of attenuation of the exiting high energy hydrogen atoms is needed in order to deduce from the NPA measurements the hydrogen flux at the source. This is done in the codes taking into account electron loss from ground and excited atomic states. Ionization and excitation of hydrogen and helium by collisions with electrons, plasma ions and bare impurity ions, Lorenz ionization, and CX with plasma and impurity ions are all taken into account. Motional Stark and Zeeman effects are

taken into consideration in describing energy levels of fast hydrogen and helium atoms in the plasma.

The atomic data base used is described in [26,27]. The only difference is the use of scalings for ionization and excitation by electrons of helium from the ground state[28] and for electron loss from the ground state of helium due to interaction with impurities[29].

The accuracy of calculation of attenuation of NBI atoms or high energy hydrogen atoms is determined mainly by uncertainty in spatial impurity ion density distribution. We have tested this accuracy by varying the impurity composition and effective charge of the plasma, using a uniform distribution $Z_{eff}$ $(0 \leq r/a \leq 1) = 2$, and one with $Z_{eff}$ $(r/a \leq 0.5) = 4$ and $Z_{eff}$ $(r/a > 0.5) = 2$. Two impurities, C and Be, were considered in giving these $Z_{eff}$ profiles, the ratio of C and Be densities was varied for each $Z_{eff}$ profile. For plasmas with $\bar{n}_e = 2.5 \times 10^{19}$ $m^{-3}$ we obtained the following variation in attenuation factors: 8% for 120kV helium NBI, 15% for 130kV deuterium NBI and 10-30% for 0.3-1 MeV hydrogen atoms. The sensitivity to impurity content is highest for 0.2-0.3 MeV hydrogen atoms because cross-sections for hydrogen ionization and excitation by impurity ions are largest in this energy interval.

Fig.11 also shows the He atom density at the plasma center due to 6MW of 120 kV helium NBI at oct.4. We obtain the result that the density of [H] ions of the main impurity species is comparable to that of injected helium atoms.

**3. Atomic density at plasma core due to NBI halo:**

A 3-D Monte Carlo code was developed to calculate halo atom density distributions in the plasma due to deuterium and helium neutral beam injection. The code describes beam attenuation, creation and propagation of halo atoms, taking into account all atomic processes mentioned above. Fig.12 shows an example of deuterium halo atom distribution calculated for a plasma with $\bar{n}_e = 2 \times 10^{19}$ $m^{-3}$ . Fig.13 shows relative contribution of the halo to the total proton neutralization probability $P_V$ for plasmas with three different $\bar{n}_e$. The calculation was performed with a total of 11.6 MW of 130 kV deuterium NBI from oct.4 and oct.8, where the relative proportion of NBI from the two octants was varied. The variation with proton energy in the halo contribution to proton neutralization arises from variation in NBI power from the two octants. We see that the halo contribution is <10% at $\bar{n}_e < 4 \times 10^{19}$ $m^{-3}$ but becomes larger and important at $\bar{n}_e \geq 6 \times 10^{19}$ $m^{-3}$.

## 4.2 Determination of $\Lambda$ and of background thermal deuterium density $n_d$ at the plasma core from ratio of measured hydrogen fluxes

The procedure for inferring the parameter $\Lambda = 1/\tau_Z + \beta_Z . n_d$ and thereby the thermal deuterium density $n_d$ is based on the fact that the proton neutralization and flux to the NPA are governed by the density of [H] ions of the main plasma impurities, which in turn is sustained by the density of deuterium atoms in the plasma.

1. We shall first consider a plasma with only one impurity. Consider that we measure the hydrogen flux $\Gamma(E_i)$ at two close time points t1 and t2 in which at t2 a controlled increase $n_d$ in deuterium atom density is effected using NBI. Using eq.9 we can then express the ratio of fluxes at times t1 and t2 as

$$\left[\Gamma(E_i,t1)/\,\Gamma(E_i,t2)\right] \approx \left[(n_{Z-1})_{t1} / (n_{Z-1})_{t2}\right]$$

$$\approx\left[\{\Lambda+(\alpha_Z n_e)_{t1}\}/\{\Lambda+(\alpha_Z n_e + n_b \gamma_b <\sigma v>^{b}_{CX})_{t2}\}\right].\left[(n_Z)_{t1} / (n_Z)_{t2}\right].\left[(I_{Z-1}\, n_e)_{t2} /(I_{Z-1}\, n_e)_{t1}\right] \quad \text{eq.13}$$

Defining $\chi = \{ (n_Z)_{t2} (I_{Z-1}\, n_e)_{t1} \} / \{ (n_Z)_{t1} (I_{Z-1}\, n_e)_{t2} \}$ we obtain that

$$\Lambda=\{(\alpha_Z n_e + n_b \gamma_b <\sigma v>^{b}_{CXZ)t2} . \chi . \Gamma(E_i,t1)/\Gamma(E_i,t2) - (\alpha_Z n_e)_{t1}\} / \{1-\chi . \Gamma(E_i,t1)/\Gamma(E_i,t2)\} \quad \text{eq.14}$$

The best way to determine parameter $\Lambda$ is by making $\chi = 1$ by choosing (t2-t1) « ($\tau_Z$ and $\tau_S$), where $\tau_Z$ is the impurity ion confinement time defined earlier and $\tau_S$ is the sawtooth repetition period. This then excludes any dependence of $\Lambda$ on impurity density.

In eq.13 and eq.14 we have assumed that $\Lambda$ remains constant between t1 and t2. This assumption is not restrictive because $\Lambda$ is important in determining only the "passive" flux. For the "active" flux, arising with NBI at oct.4, CX by bare impurity ions with beam atoms is much more important than processes described by $\Lambda$, in other words in this case $\Lambda$ can be omitted in the denominator in eq.13.

The accuracy of $\Lambda$ thus obtained is determined by uncertainties in the main terms in eq.14. When (t2 - t1 ) « ($\tau_Z$ and $\tau_S$), we obtain that typically $\delta(n_b) = 15\%$, $\delta(<\sigma v>^{b}_{CXZ}) = 20\%$ [4], and $\delta[\Gamma(E_i, t1)/\Gamma(E_i, t2)] = 10\%$. Then $\delta(\Lambda) \cong 30\%$.

For JET plasmas the simplified model considered here is most accurate for measurements of $f(E_P)$ for proton energy $E_P$ >0.6 MeV/u. This is so because carbon impurity ions make the dominant contribution to proton neutralization at such energies. More about this in section 4.3.

2. In general several different impurity donors may contribute equally to proton neutralization. Then in place of single unknown parameter $\Lambda$ we have to consider two unknown parameters $n_d$ and $\tau_Z$. Then the modeling is possible in the following situations:

a. At high level of NBI the rate of direct CX between bare impurity ions and NBI atoms can be made to far exceed the rate of other processes competing to reduce the impurity ionization level. Then, keeping only CX with NBI atoms in eq.9, the hydrogen flux from the plasma to the NPA can be modeled with 20% accuracy, for ≥5MW NBI level.

b. In the absence of NBI when in eq.9 either the impurity ion transport term or the term describing CX between protons and thermal deuterium atoms becomes dominant, in other words when $1/\tau_Z \ll \beta_Z n_d$ or when $1/\tau_Z \gg \beta_Z n_d$ . In JET the former is most likely because of observed long impurity confinement time in the plasma center for most plasma modes[30].

We shall estimate minimum absolute value of $\tau_Z$ in JET from existing knowledge of impurity transport[30,31]. The radial impurity ion flux $\Gamma_Z$ and impurity ion confinement time $\tau_Z$ in the plasma center are commonly described by the model

$$\Gamma_Z = -Dn'_Z + r/a \,.\, V \,.\, n_Z \qquad \text{and} \qquad \tau_Z = n_Z/\mathrm{div}\,\Gamma_Z \qquad \text{eq.15}$$

Usually $D(m^2/s) = (0.03 \text{ to } 0.15)$ and $V(m/s) = -(0.1 \text{ to } 0.6)$, as in [31].

Then $$\tau_Z = -n_Z \,.\, r \,/\{D \,.\, n_Z' + D \,.\, r \,.\, n_Z'' - V \,.\, n_Z \,.\, r/a \,(r \,.\, n_Z'/n_Z + 2)\} \qquad \text{eq.16}$$

Because $|\, n_Z' \,| \gg r \,.\, |\, n_Z'' \,|$ in the plasma center, we omit the second term in the denominator of eq.16. Spectroscopic measurements show that the spatial profile of bare light impurity ions in JET is wide, allowing us to assume that $n_Z'/n \cong -1/a$, where the minor radius of the plasma a=1m usually. The last term in the denominator is positive therefore we obtain, after averaging $\tau_Z$ over the observed plasma volume along the NPA line-of-sight (for $\tau_Z$ >0)

$$\bar{\tau}_Z > a\Delta Z/2D \qquad \text{eq.17}$$

where $2\Delta Z$ is the vertical extent of the observed plasma volume. Taking maximum values for coefficients D, $D = 0.15 m^2/s$, and using $a = 1m$ and $\Delta Z = 0.3m$ we find that in all cases $\bar{\tau}_Z > 1s$. Measurements of evolution of radial helium density profiles have yielded confinement times for $He^{2+}$ close to 0.5s [32], making the CX term containing $n_d$ become dominant for $n_d > 10^{13} m^{-3}$.

In such a case we determine the parameter $n_d$ as follows. Fig14 shows evolution of the main parameters in pulse #27325, a deuterium plasma with $B\phi = 2.9T$, $I\phi = 2.7$ MA which was heated with $\cong$ 6MW of ICRF power in the D(H) heating mode and $\cong$ 7.5MW of NBI power at oct.8 in the form of 130kV deuterium atoms. We have determined $\bar{f}(E_P)$ at two time points t1 and t2 such that $(t2-t1) \ll (\tau_Z$ and $\tau_S)$. During this interval key parameters determining $f(E_P)$ due to ICRF heating remained constant. We may then assume that $\bar{f}(E_P)$ also was unchanged from t1 to t2. Keeping $\bar{\tau}_Z$ constant we iterated $n_d$, the background thermal deuterium atom density, to obtain a match of $\bar{f}(E_P)$ at times t1 and t2. Fig.15 shows the result.

Using $\tau_Z = 1s$ the best match between $\bar{f}(E_P)$ at t1 and t2 was obtained with the background thermal deuterium density $n_d = 1.5 \times 10^{13}$ $m^{-3}$. Fig.16 shows how the inferred value of $n_d$ depends on $\tau_Z$. We see that $n_d$ can be determined to within $\pm$ 25% when $\tau_Z \geq 0.5s$.

Lastly, we have tested the effect of varying the proportion of C and Be impurity density on the accuracy of inferred $n_d$ . The density of $C^{6+}$ and $Be^{4+}$ was measured using CX spectroscopy with an accuracy of $\pm$ 30%. This uncertainty gives a variation in deduced value of $n_d$ of less than 10%. The total accuracy of inferred $n_d$ is 40%, taking into account all the uncertainties arising in the determination of $\Lambda$. The procedure described above for determination of $n_d$ is an important new diagnostic application of the high energy hydrogen flux measurement.

### 4.3 Total proton neutralization probability

Fig.17 shows different contributions to total proton neutralization probability in a typical JET plasma pulse with ICRF and NBI heating. These contributions consist of those due to (i) [H] and [He] ions of C, and Be, (ii) [H] ions of He and thermal He atoms, (iii) background thermal deuterium and NBI atoms, (iv) electrons. The data shown in fig.17 characterizes the main result to date of the model developed and analysis presented here, that is

1. CX with [H] ions of the main impurities is the dominant neutralization process for MeV protons in JET plasmas. C, Be and He impurity ions cause the neutralization probability to increase by two orders of magnitude above that due to CX with NBI and background

atoms, and that due to radiative recombination. This allows measurement of MeV energy protons in JET plasmas without recourse to NBI.

2. In the low density JET plasmas injection of atomic beams anywhere in the plasma causes a large increase in the density of [H] impurity ions at oct.4. The "active" flux detected in the experiments arises mainly from increase in [H] impurity donor ion density due to NBI, as seen in fig.11. In JET this is the dominant CX process at $E_P$ >0.5 MeV/u.

3. In usual JET plasmas carbon is the most abundent impurity and the proton neutralization probability is dominated by [H] carbon donors, for $E_P$ >0.6 MeV/u. This is the most favourable condition for an accurate determination of $f(E_P)$.

### 4.4 Description of the measured hydrogen flux using IIN modeling

**1. After pellet injection**

We reconsider pulse #27325 shown in fig.14. Soon after time t2, despite constant ICRF and NBI power, a fast reduction of fluxes in all NPA channels occurs. This comes about because of injection of a small shallow penetrating deuterium pellet into the plasma. The pellet event gives a sharp increase in edge electron density which is seen in Thomson scattering measurements, and a sharp reduction of $T_e(0)$ due to the pellet or a concomitant giant sawtooth crash.

In modeling the hydrogen flux we use bare Be ion density ($\cong$7% of $n_e$) reliably measured at time t2 using CX spectroscopy and add bare C ion density to give the measured $Z_{eff}$ at t2. We describe the subsequent evolution of impurity donor densities by keeping constant the ratio of number of bare Be and C ions and using the behaviour of $Z_{eff}$ to scale their absolute densities.

Assuming that $f(E_P)$ remains constant in pulse #27325 from t = 8.8s until soon after pellet injection, IIN modeling, marked by solid points in fig.14, shows that the observed reduction in hydrogen flux to the NPA after pellet injection is caused by a combination of:

a. Reduction of density of [H] impurity donors. The density of donors is maintained by electron transfer from deuterium atoms to bare impurity ions on the one hand and ionization of [H] donor ions by electrons. Due to reduction in $T_e$ at pellet njection the rate for the former process decreases whereas for the latter process it increases giving a fast reduction in density of [H] donor ions in the plasma core.

b. Reduction in NBI atom flux to the plasma core due to increased edge electron density and increased neutral beam attenuation.

c. A slow reduction in impurity influx into the plasma core which is seen in the evolution of $Z_{eff}$ after pellet injection.

d. Increased attenuation of flux of escaping high energy hydrogen atoms.

Solid points in fig.14 and fig.18 are model results derived by taking into account above points a-d. Fig.18 shows that the model gives a fair description of flux at all measured energies. Note that the good agreement achieved above lends support to an assumption in the model that sawteeth do not cause substantial redistribution of either the high energy protons or the impurity donor ions at the plasma core.

**2. Apparent saturation of ICRF driven proton tail temperature:**

An important application of the new NPA is in interpretation of high power ICRF heating in JET. An early observation was of saturation of "tail temperature" associated with the energy distribution of hydrogen flux received by the NPA, $\Gamma(E_H)$, with increasing ICRF heating power [33](see figs.1,2,3 of this reference), and a conjecture of saturation of minority tail temparature. Fig.19 shows $f(E_P) = \bar{f}(E_P)/2\Delta Z$, the ICRF driven proton energy distribution function for pulse #27336. $\bar{f}(E_P)$ was deduced from measured hydrogen fluxes at different levels of ICRF heating power. Whereas the "tail temperature" associated with $\Gamma(E_H)$ showed saturation for ICRF power ≥6 MW, IIN modeling shows that it is due to reduction of impurity donor density during the measurement. When this is properly taken into account $\bar{f}(E_P)$ evolves as expected with increasing ICRF power at least up to 10 MW. This underlines the importance of IIN modeling developed in this paper for interpretation of the NPA measurements.

## 5. ACCURACY OF DEDUCED ION ENERGY DISTRIBUTION FUNCTION $\bar{f}(E_P)$

### 5.1 Minority proton density

The uncertainties of the major parameters determining the accuracy of donor density calculation are given in Table I, expressed in percent.

**TABLE I**

**% Uncertainty in $n_Z$, $n_b$, $\Lambda$, $I_{Z-1}$, and $\langle\sigma v\rangle$**

| | $n_Z$ | $n_b$ | $\Lambda$ | $I_{Z-1}$ | $\langle\sigma v\rangle^b_{CXZ}$ |
|---|---|---|---|---|---|
| "Passive" Flux | 30 | — | 30 | 10 | — |
| "Active" Flux | 30 | 15 | — | 10 | 20 |

Employing data of Table I we deduce that the accuracy of modeled impurity donor density is $\delta(n_{Z-1}) \approx 40\%$ in both "passive" and "active" flux cases. Taking into account 20% accuracy of

the cross-sections for CX between protons and [H] C ions, 15% accuracy for the calculation of attenuation factor for neutralized protons exiting the plasma, and 10% uncertainty in calibration of the NPA, we obtain an accuracy of ≅ 50% for deduced minority density for $E_P$ >0.6 MeV/u. Notice that in general the interpretation of "passive" flux measurements is less reliable than that of the "active" flux because of larger influence of impurity ion transport on determination of impurity donor densities in the former case.

### 5.2 Effective proton tail temperature

The proton tail temperature $T_P$ associated with $\bar{f}(E_P)$ can be determined with much greater accuracy than the density of protons in the plasma because uncertainties in $T_P$ are determined only by uncertainties in the cross-sections used. For measurements in the range $E_P$ >0.6MeV/u we have shown that $C^{5+}$ ions dominate the CX proton neutralization. The uncertainty in determining $T_P$ and $\Delta T_P/T_P$ is related to uncertainty in the corresponding CX cross-sections by

$$\Delta T_P/T_P = T_P . (-d\,ln P_V/dE_P) . (\Delta\sigma_{CX}/\sigma_{CX}) \qquad \text{eq.18}$$

Typically $(-d\,ln P_V/dE_P) \cong (1\text{-}2)\times10^{-3}$ keV$^{-1}$ for $0.5 \le E_P(\text{keV}) \le 1$. Then

$$\Delta T_P/T_P \cong 2\times10^{-3} . T_P(\text{keV}) . (\Delta\sigma_{CX}/\sigma_{CX}) \qquad \text{eq.19}$$

Fig.20 shows variation of $\Delta T_P/T_P$ with $T_P$, on the basis of the above analysis, using $\Delta\sigma_{CX}/\sigma_{CX}$ ≅ 20%, the typical uncertainty in the relevant cross-section. We see that $T_P$ can be determined with an accuracy of 10% for $T_P \le 300$ keV.

## 6. PROTON NEUTRALIZATION IN ITER PLASMAS

We have applied the IIN model discussed here to compute the proton neutralization probability in the center of ITER plasma using the forecast values for plasma parameters: $T_e = T_i = 10$ keV, $n_e = 1.5\times10^{20}$ m$^{-3}$, $n_d = 10^{12}$ m$^{-3}$, $Z_{eff} = 1.5$ made up of 20% He, 1% Be and 0.1% C impurity [34]. The IIN probability for ITER plasmas, unlike JET, depends on $\tau_Z$ due to very low density of thermal deuterium atoms. Therefore we have calculated $P_V$ for different values of $\tau_Z$ in the expected ITER range $1 \le \tau_Z(s) \le 20$ [36]. Results of the computation are presented in fig.21. We conclude that IIN will be dominant in ITER plasmas at E<1MeV/u. Notice that if carbon were increased to 1% of electron density then IIN will become a major neutralization process up to $E_P = 1.5\div2$ MeV/u depending on the value of $\tau_Z$.

We have estimated the hydrogen flux from ITER plasmas without NBI and the expected count rate for the parameters of the NPA used on JET. We have assumed ICRF heating with relative hydrogen minority density to be as in JET, using parameters given in Table II.

**TABLE II**

**Setup Parameters for Simulation of Hydrogen Flux from ITER**

| | $L_{NPA}$(m) | $\Omega_{NPA}$ (st) | V($m^3$) | $\bar{n}_e a$ ($m^{-2}$) |
|---|---|---|---|---|
| JET | 6.4 | $1.2\times10^{-6}$ | 0.05x0.05x0.6 | $3\times10^{19}$ |
| ITER | 13 | $3\times10^{-7}$ | 0.5x0.5x0.5 | $3\times10^{20}$ |

$L_{NPA}$ is the distance from the NPA to the plasma center, $\Omega_{NPA}$ is the solid-angle of observation, V is the observed interaction volume in the plasma, and $\bar{n}_e a$ is the line-integrated plasma density. We have assumed that the NPA is located in the horizontal mid-plane of ITER and thus plasma elongation is not explicitly included.

Table III gives the neutralization probability $P_\gamma$ and attenuation factors $\gamma$ for exiting hydrogen, and count rate $N_C$ for hydrogen flux received into the NPA, for "passive" flux measurements in JET and the expectation for similar measurements on ITER plasmas, using $\tau_Z = 2.5$s.

**TABLE III**

**Transparancy, Neutralization Probability and Count rate in JET and ITER**

| | JET | | | ITER | | |
|---|---|---|---|---|---|---|
| E(MeV/u) | $\gamma$ | $P_\gamma(s^{-1})$ | $N_C(s^{-1})$ | $\gamma$ | $P_\gamma(s^{-1})$ | $N_C(s^{-1})$ |
| 0.3 | 0.57 | $4.3\times10^{-2}$ | $4.5\times10^{3}$ | $2.7\times10^{-2}$ | $6\times10^{-2}$ | $3.5\times10^{4}$ |
| 0.5 | 0.69 | $2.1\times10^{-2}$ | $1\times10^{4}$ | $6.7\times10^{-2}$ | $1\times10^{-2}$ | $5\times10^{4}$ |
| 1.0 | 0.79 | $9\times10^{-3}$ | $1\times10^{3}$ | $2.2\times10^{-1}$ | $2.6\times10^{-3}$ | $8\times10^{3}$ |

These estimates show that the proton neutralization probability in the core of ITER plasmas will be large enough to give measurable hydrogen flux without recourse to NBI for charge donors. Nevertheless NBI in ITER will be required for CX spectroscopy measurements of absolute impurity densities which are necessary for deduction of absolute $f(E_P)$.

# 7. CONCLUSIONS

1. The flux of MeV energy hydrogen atoms from JET plasmas, measured with a high energy NPA, has been described using the Impurity Induced Neutralization(IIN) model. This shows that charge-exchange with hydrogen-like ions of main plasma impurities is the dominant neutralization process for high energy protons in the plasma.

2. The most accurate measurement of parameters of the proton energy distribution function is obtained in the energy range $E_P > 0.6$ MeV/u when hydrogen-like ions of carbon are the main CX donors in IIN.

3. A model describing neutralization of protons with energy $E_P > 100$ keV/u has been developed. The model includes atomic processes which allow diagnostic application of the high energy NPA for a wide range of plasma parameters. Atomic hydrogen, consisting of background thermal atoms, NBI atoms and halo atoms arising in dense plasmas due to NBI, are all included in the model. Calculation of enhanced attenuation, of both NBI atoms and MeV energy hydrogen atoms exiting the plasma, due to electron loss through excited states is also included.

Analysis shows that at $\bar{n}_e \leq 4 \times 10^{19}$ m$^{-3}$, for NPA measurements in the energy range $E_P > 0.5$ MeV/u, the effective tail temperature $T_P$ associated with the proton energy distribution function can be determined with better than 10% accuracy for $T_P < 300$ keV. Accuracy of determination of the minority proton density is estimated to be 50%. For more reliable inference of proton density more precise values for cross-sections for CX between protons and $Be^{3+}$ and $C^{5+}$ ions are required. Computation of such accurate cross-sections is in hand.

4. A new method for determination of thermal deuterium density $n_d$ in the core of JET plasmas is developed. It is based on comparison of the "passive" hydrogen flux with that when a controlled change is made in the central neutral density using NBI. In the plasma core radial impurity ion transport typically makes an insignificant contribution to ion charge-state balance. Then this method yields $n_d$ with $\approx 40\%$ precision when $\bar{n}_e \leq 4 \times 10^{19}$ m$^{-3}$.

5. IIN modeling predicts that it will be a major neutralization process for hydrogenic ions in ITER at $E \leq 1$MeV/u. Using an NPA with parameters close to those of the NPA used on JET, our estimations show that measurement of flux of neutralized ICRF driven protons will be possible in ITER without recourse to injection of atomic beams.

## 8. ACKNOWLEDGEMENTS

The authors are grateful to M.S.Samsonov for assistance in writing the Monte Carlo code for calculation of halo density and to A.J.Stuart for inplementing it on JET, to M.von Hellermann and R.König for analysis of accuracy of CX spectroscopy measurements of bare impurity ion densities, to P.van Belle for assistance with orbit calculations, to R.Giannella for discussions on impurity transport, and to P.R.Thomas for his interest and support of this work.

# 9. REFERENCES


[1] KOROTKOV, A.A. and GONDHALEKAR, A., Proceedings of 21st EPS Conference on Controlled Fusion and Plasma Physics, Montpellier, 1994. Europhysics Conference Abstracts 18B(1994)I-266.

[2] IZVOZCHIKOV, A.B., KHUDOLEEV, A.V., PETROV, M.P., et al., JET Report, JET-R(1991)12.

[3] PETROV, M.P., AFANASYEV, V.I., CORTI, S., et al., Proceedings of 19th EPS Conference on Controlled Fusion and Plasma Physics, Innsbruck, 1993. Europhysics Conference Abstracts 16C(1992)II-1031.

[4] BARNETT, C.F. (Editor), Oak Ridge National Laboratory Reports, Atomic Data for Fusion, Vol.1 ORNL-6086/VI (1990), and Vol.5 ORNL-6090(1990).

[5] BETHE, H.G. and SALPETER, E.E., Quantum Mechanics of One- and Two-Electron Atoms, Springer Verlag, Berlin (1957).

[6] SOLOV'EV, E.A., Soviet Physics Uspekhi, 32(1989)228.

[7] SOLOV'EV, E.A. and KOROTKOV, A.A., to be published.

[8] RINN, K., MELCHERT, F., RINK, K. and SALZBORN, E., Journal of Physics B18(1985)3783.

[9] PEART, B., RINN, K. and DOLDER, K.T., Journal of Physics B16(1977)2675.

[10] WATTS, M.F., DUNN, K.F. and GILBODY, H.B., Journal of Physics B19(1986)L335.

[11] WINTER, T.G., Phyical Review A35(1987)3799.

[12] FRITSCH, W. and LIN, C.D., Journal of Physics B15(1982)1255.

[13] ERREA, L.F., GOMEZ-LLORENTE, J.M., MENDEZ, L. and RIERA, A., Journal of Physics B20(1987)6089.

[14] WINTER, T.G. and ALSTON, S.G., Physical Review A45(1992)1562.

[15] MUKHERJEE, S. and SIL, N.C., Journal of Physics B13(1980)3421.

[16] CROTHERS, D.S.F. and DUBE, L.J., Advances in Atomic, Molecular and Optical Physics, 30(1993)287.

[17] GROZDANOV, T.P. and KRSTIC, P.S., Physics Scripta 38(1988)32.

[18] TAULBJERG, K., BARRACHINA, R.O. and MACEK, J.H., Physical Review A41(1990)207.

[19] MACEK, J.H. and ALSTON, S.G., Physical Review A26(1981)250.

[20] BRANSDEN, B.H. and DEWANGAN, D.P., Advances in Atomic, Molecular and Optical Physics, 25(1988)343.

[21] CROTHERS, D.S.F. and DUNSEATH, K.M., Journal of Physics B20(1987)4115.

[22] CROTHERS, D.S.F., Journal of Physics B18(1985)2893.

[23] KUANG, YU.R., Journal of Physics B25(1992)199.

[24] BURGESS, A. and TWORKOWSKI, A.S., Astrophysical Journal 205(1976)L105.

[25] BOILEAU, A., von HELLERMANN, M. G. and HORTON, L. et. al., Nuclear Fusion 29(1989)1449.

[26] JANEV, R.K., BOLEY, C.D. and POST, D.E., Nuclear Fusion 29(1989)2125.

[27] KOROTKOV, A.A., Nuclear Fusion A + M Supplement 3(1992)79.

[28] KATO, T. and JANEV, R.K., Nuclear Fusion A + M Supplement 3(1992)33.

[29] JANEV, R.K., Nuclear Fusion A + M Supplement 3(1992)71.

[30] GIANNELLA, R., HAWKES, N.C., LAURO-TARONI, L., et al., Plasma Physics and Controlled Fusion 34(1992)687.

[31] PASINI, D., MATTIOLI, M., EDWARDS, A.W., et al., Nuclear Fusion 30(1990)2049.

[32] von HELLERMANN, M., BARTH, K., BICKLEY, A.J., et al., Proceedings of 22nd EPS Conference on Controlled Fusion and Plasma Physics, Bournemouth, July 1995. Europhysics Conference Abstracts, 19C(1995)II-9.

[33] KHUDOLEEV, A.V., AFANASYEV, V.I., CORTI, S., et al., Proceedings of EPS Topical Conference on RF Heating and Current Drive of Fusion Devices, Brussels, 1992. 16E(1992)117.

[34] ITER Physics and Plasma Operation Studies. ITER TAC Meeting Report, ITER TAC-3-03(1993).

[35] KOROTKOV, A.A. and ZINOV'EV, A.N., Soviet Journal of Plasma Physics, 15(1989)136.

[36] KOROTKOV, A.A. and ERMOLAEV, A.M., Proceedings of 22nd EPS Conference on Controlled Fusion and Plasma Physics, Bournemouth, 1995. Europhysics Conference Abstracts, 19C(1995)III-389.

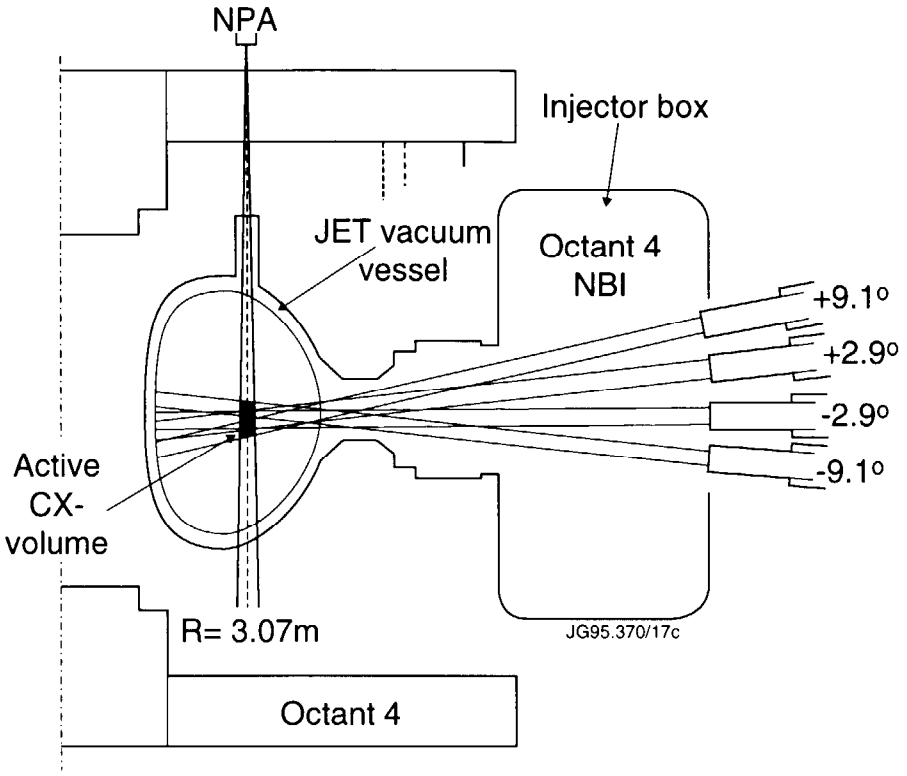


Fig.1: Experimental setup showing cross-section of the JET torus. The NPA was located at the top of the torus with its vertical line-of-sight intersecting octant-4 neutral beams in the plasma core region at major radius R=3.07m. The Doppler broadened ICRF resonance was usually coincident with the NPA line-of-sight.

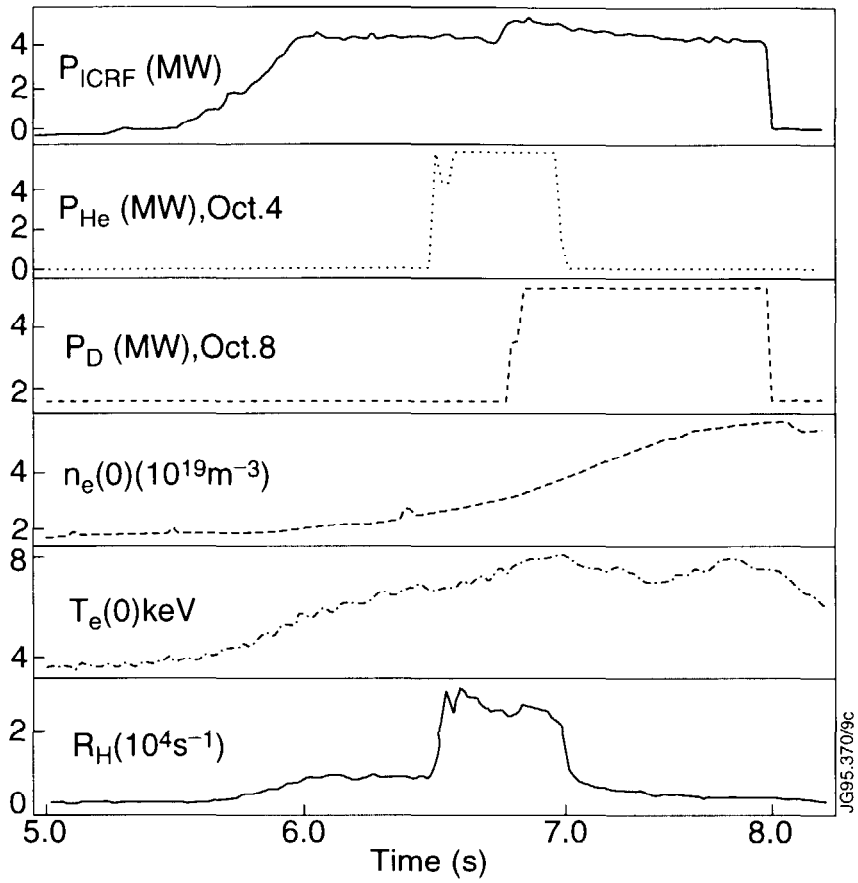


Fig.2: Observations of "passive" and "active" hydrogen fluxes in D(H) ICRF heating experiments. Traces show evolution of $P_{ICRF}$, $P_{NBI}$ from oct.8 and oct.4, $n_e(0)$, $T_e(0)$, and count rate $R_H$ of hydrogen flux in the NPA channel for 0.42 MeV. The latter shows that good statistical accuracy in the flux measurements could be achieved.

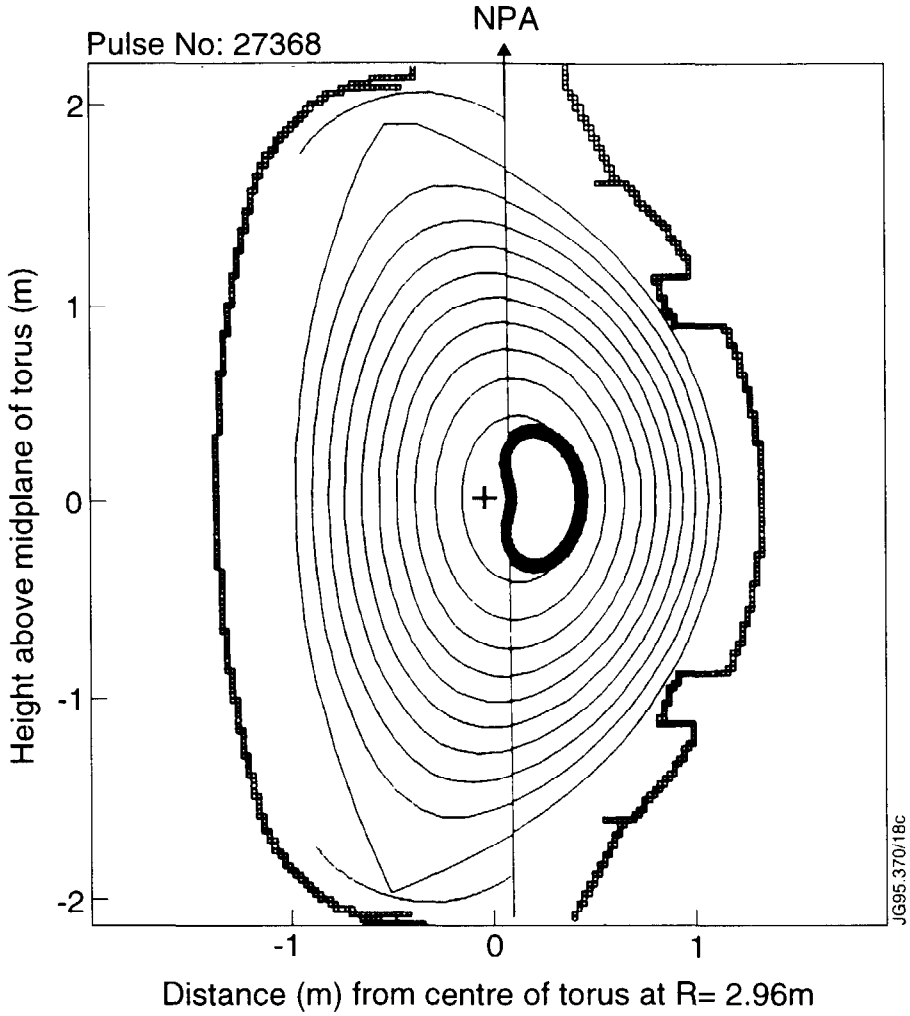


Fig.3: Poloidal cross-section of the JET torus showing the magnetic configuration of the plasma. Shown in heavy line is the poloidal projection of orbit of 0.5MeV proton with $v_Z/v_\phi = 2x10^2$ with its banana-orbit tip located on the NPA line-of-sight and inside the ICRF deposition region.

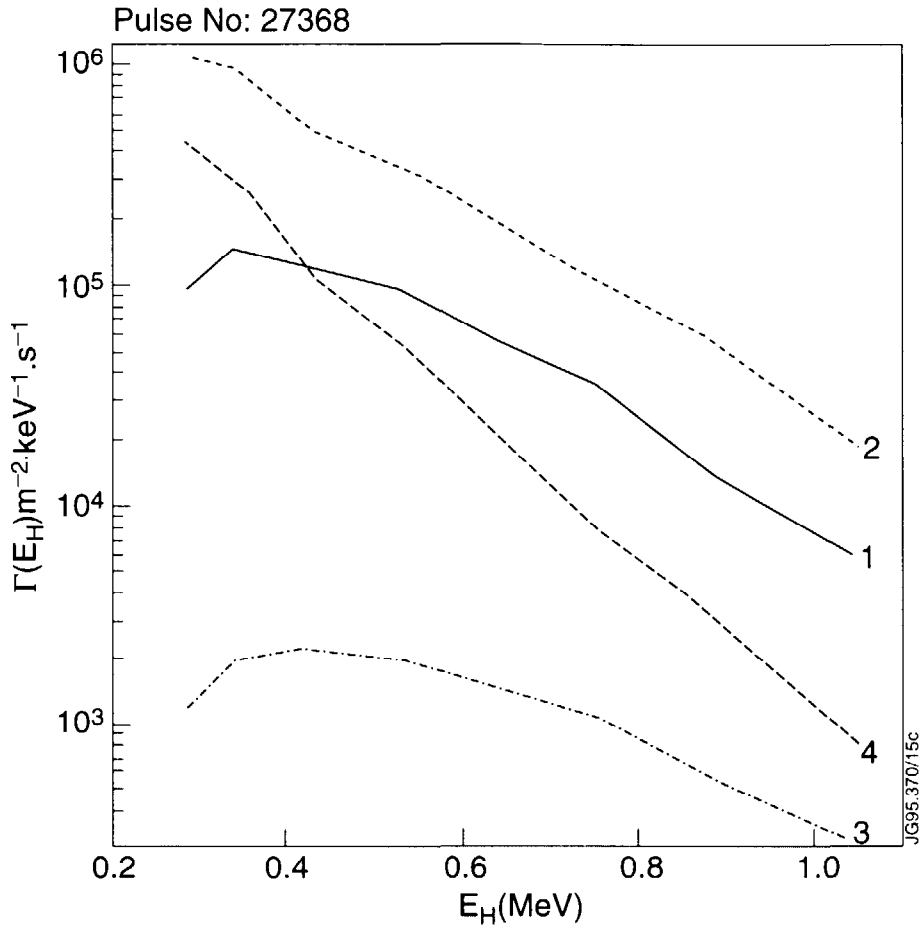


Fig.4: Energy distribution of hydrogen flux in the NPA solid angle for: (#1) measured "passive" flux at t=6.4s, (#2) measured "active" flux at t = 6.6s, (#3) modeled flux that would have arisen if radiative recombination were the only process giving rise to the "passive" flux, (#4) modeled flux that would have arisen if direct CX with injected beam atoms were the only mechanism giving the "active" flux.

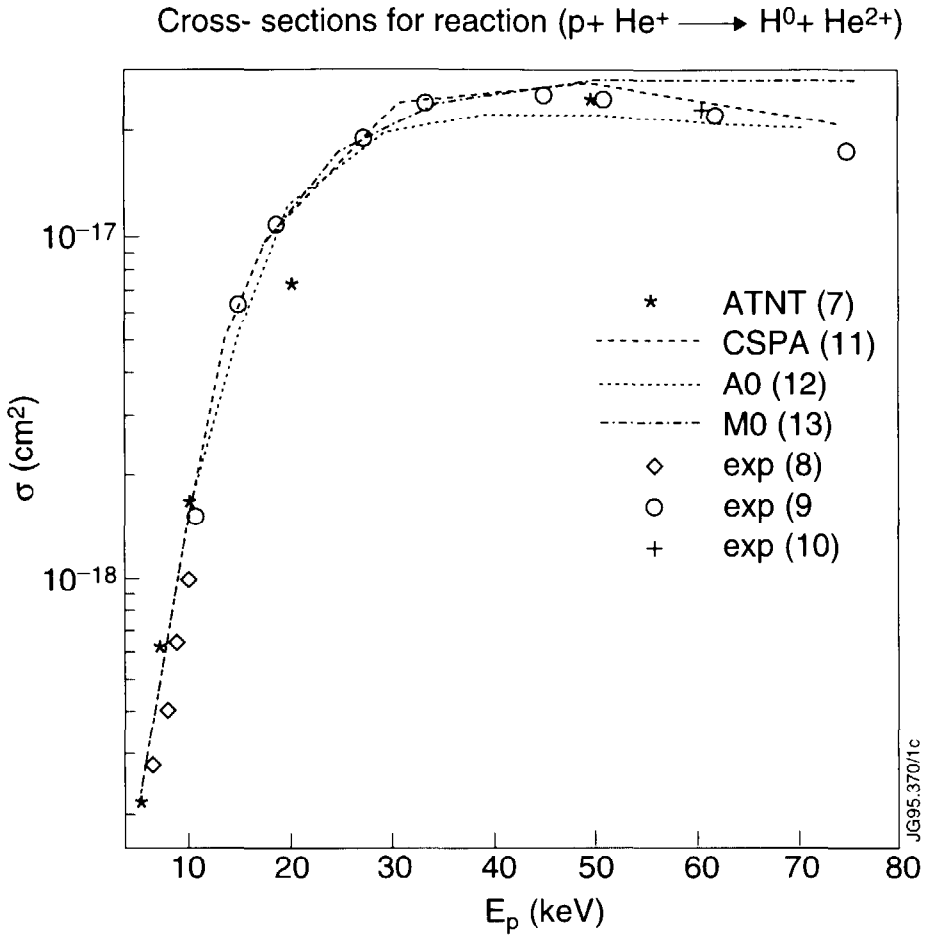


Fig.5: Comparison of different calculations of CX cross-section for the reaction ($p + He^+ \rightarrow H^0 + He^{2+}$) with measured values, in the low energy ($v \ll Z$) range. Calculations shown are using ATNT[7], CPSA[11], AO[12], and MO[13]. Measurements shown are from [8,9,10].

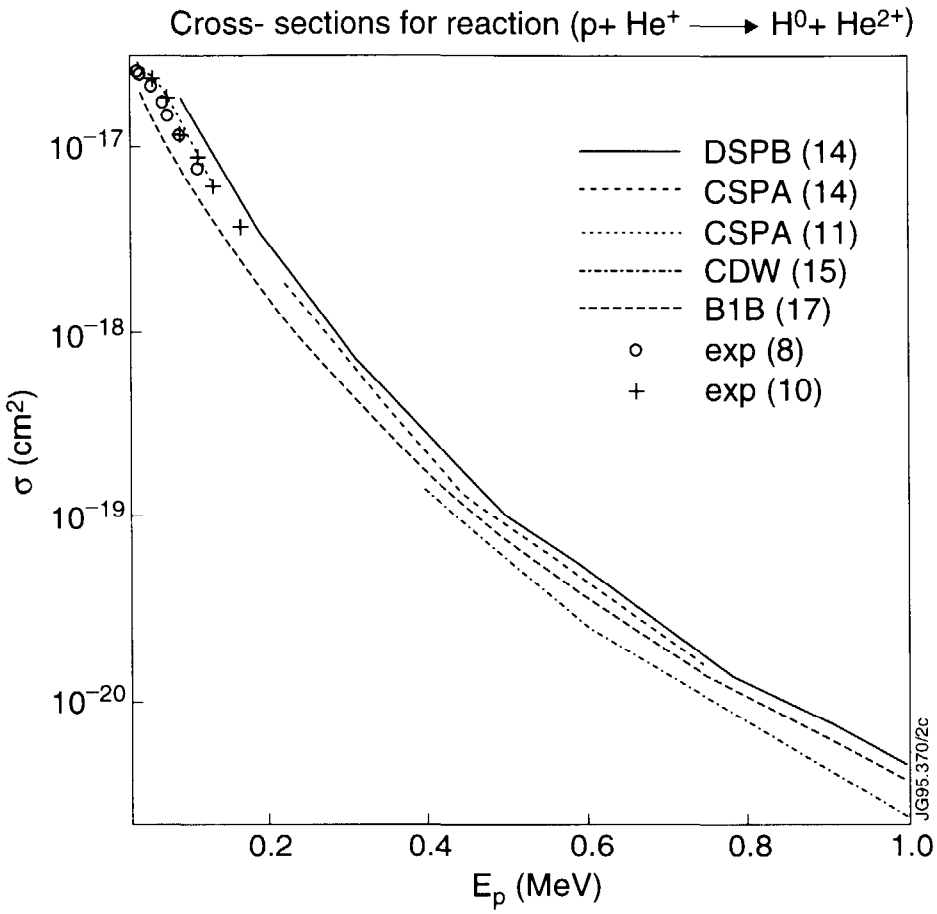


Fig.6: Comparison of different calculations of CX cross-section for the reaction ($p + He^+ \rightarrow H^0 + He^{2+}$) with measured values, in the high energy (v>Z) range. Calculations are using DSPB[14], CSPA[14], CSPA[11], CDW[15], and B1B[17]. Measurements are from [8,9].

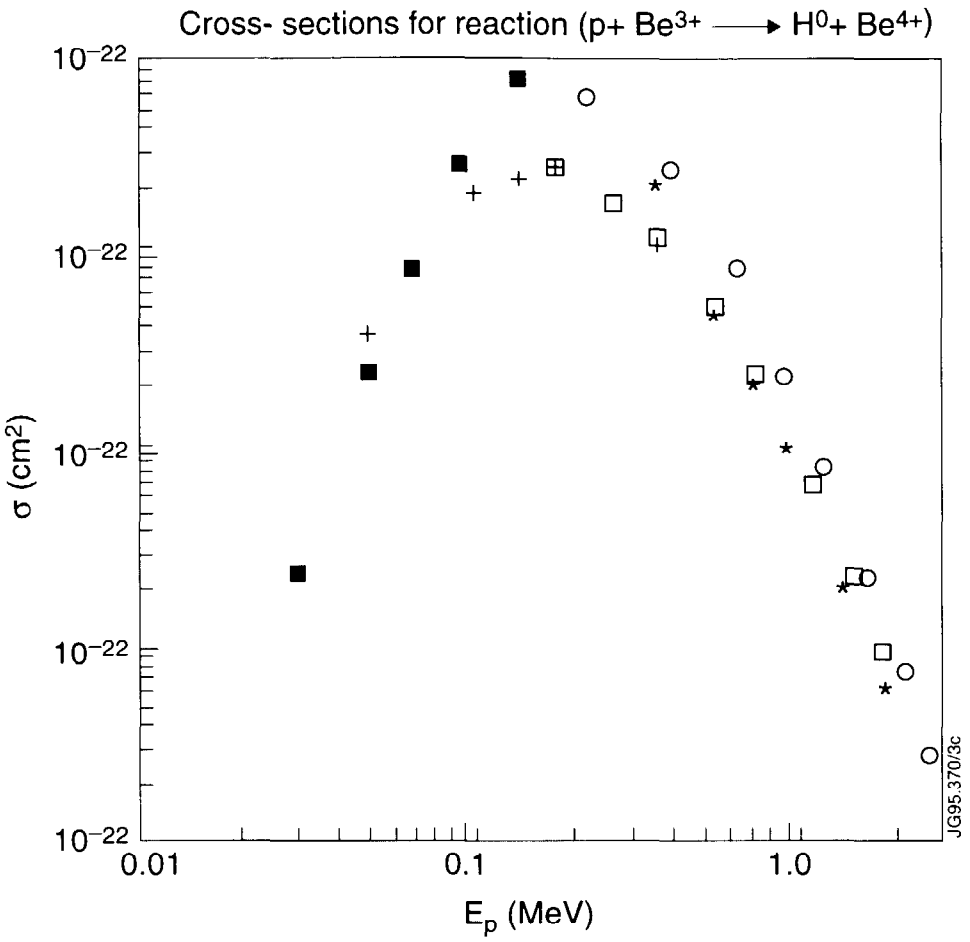


Fig.7: Comparison of results of calculations of CX cross-sections for the reaction ($p + Be^{3+} \rightarrow H^{0} + Be^{4+}$) using different methods: ■ATNT[7], + CPSA[11], B1B[17], * CDW[15], o DSPB [18].

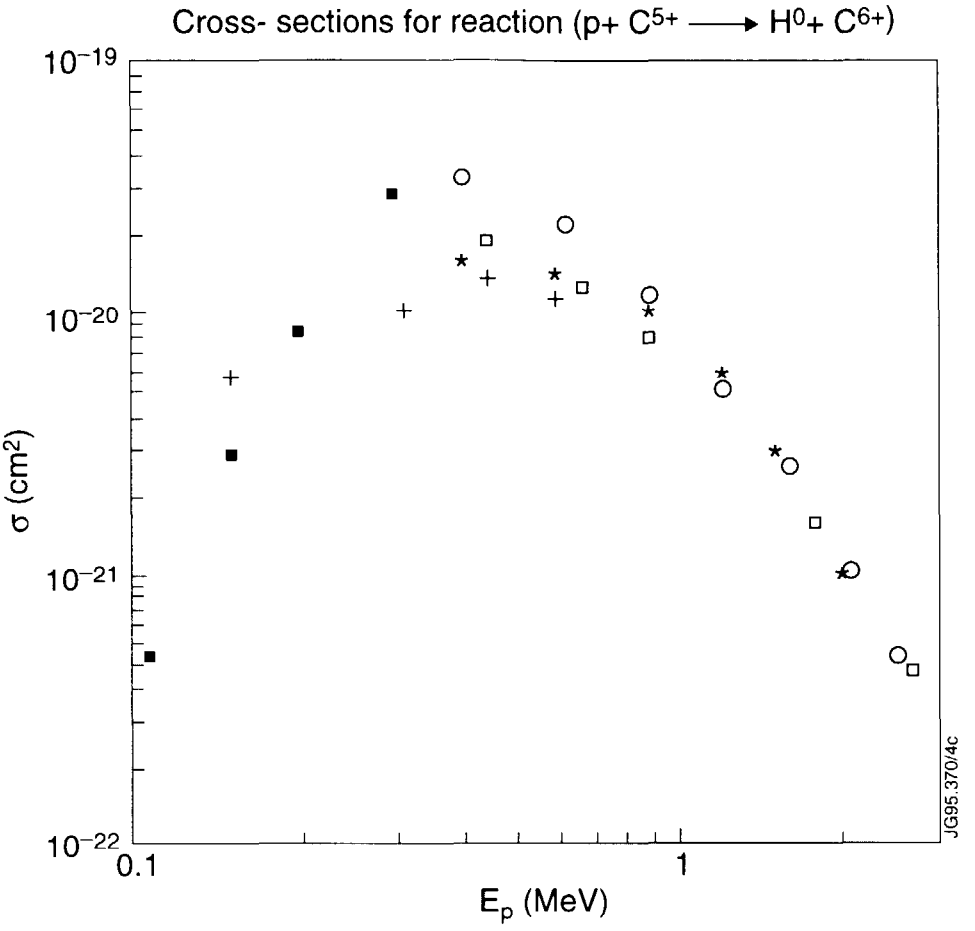


Fig.8: Comparison of results of calculations of CX cross-sections for the reaction ($p + C^{5+} \rightarrow H^0 + C^{6+}$) using different methods: ■ ATNT[7], + CPSA[11], B1B[17], * CDW[15], o DSPB [18].

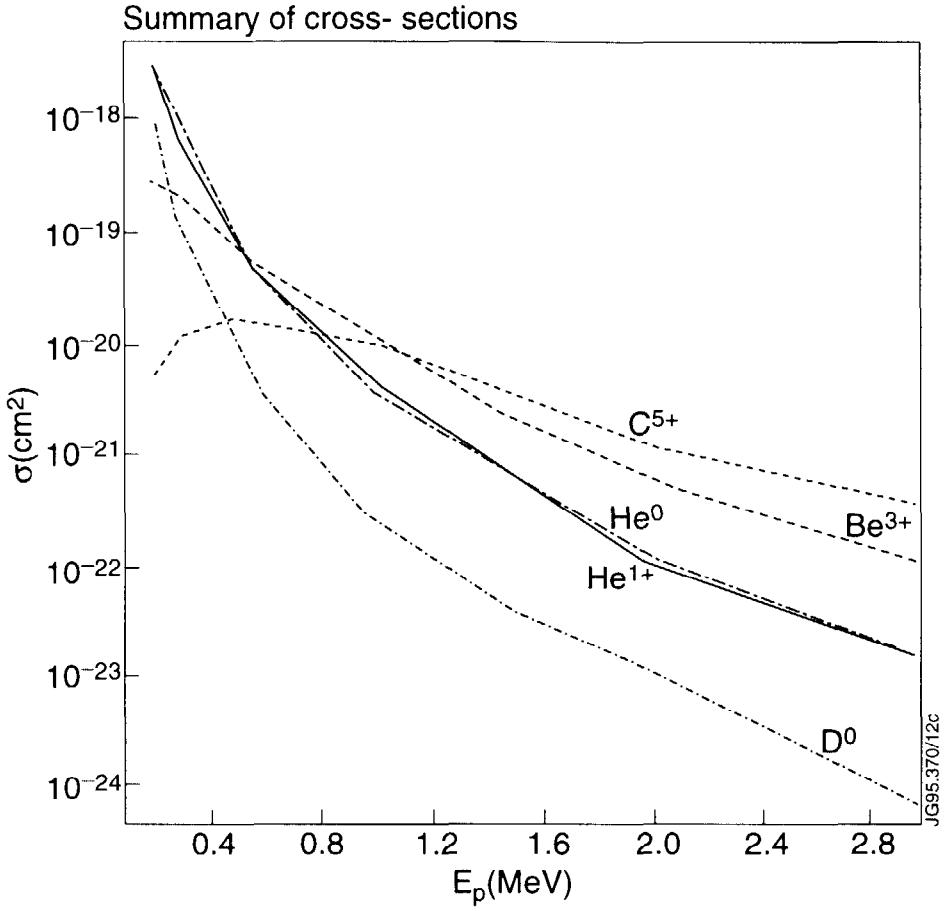


Fig.9: Summary of comparison of cross-sections for CX by protons with atoms of D and He, and with [H] impurity ions $He^{+}$, $Be^{3+}$, $C^{5+}$. Note that for $E_P$(MeV)>0.5 the cross-sections for CX with [H] ions of Be and C are larger than those for CX with D and He atoms.

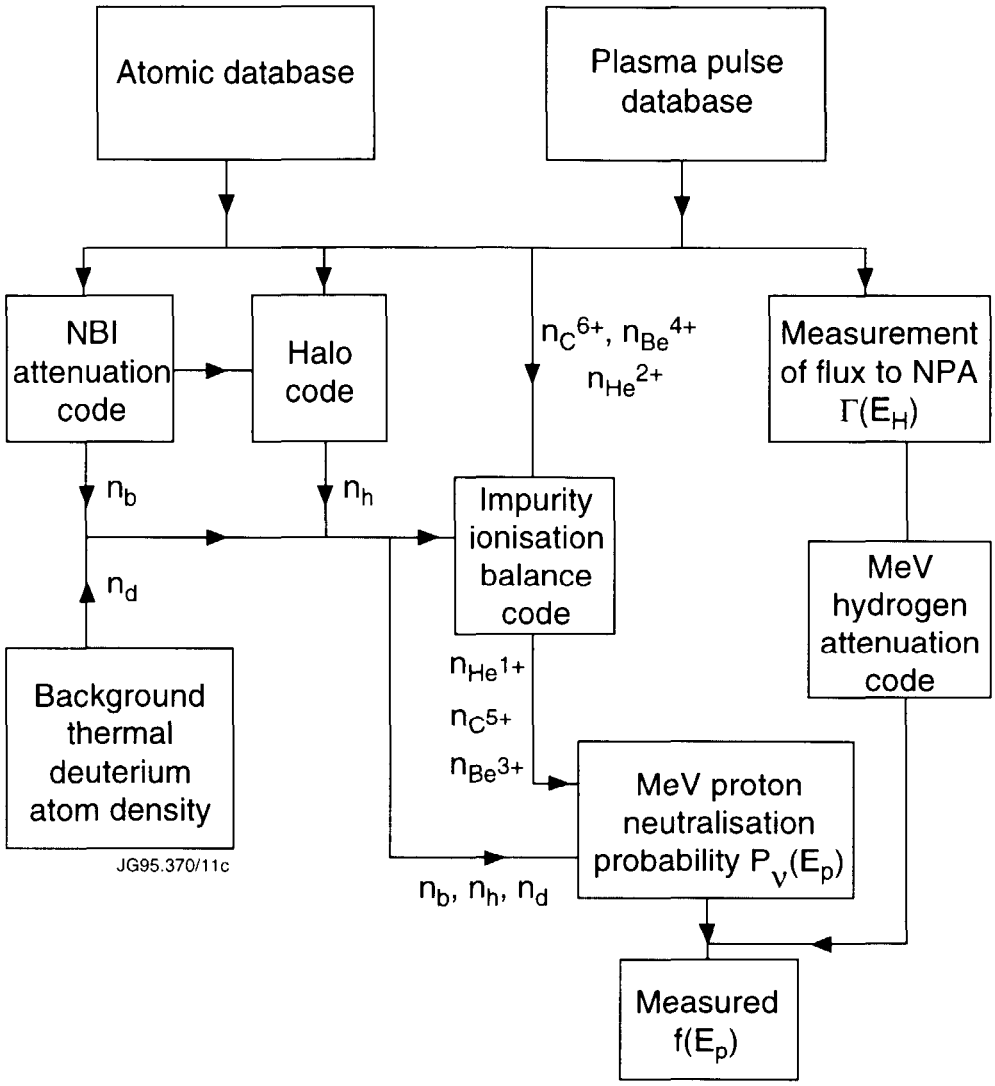


Fig.10: Schematic organization of codes used for modeling the measured hydrogen flux and deduction of $\bar{f}(E_P)$. The codes draw CX cross-sections from an atomic data base, nuclear impurity ion densities $n_C$, $n_{Be}$, and $n_{He}$, and $T_e$, $n_e$ and $Z_{eff}$ and other data from the JET Processed Pulse Files (PPF), and NPA details from the JET Pulse Files (JPF). The codes calculate $n_b$, $n_h$, and [H] and [He] impurity ion densities for C, Be and He, the total proton neutralization probability $P_V(E_P)$ and the distribution function $\bar{f}(E_P)$.

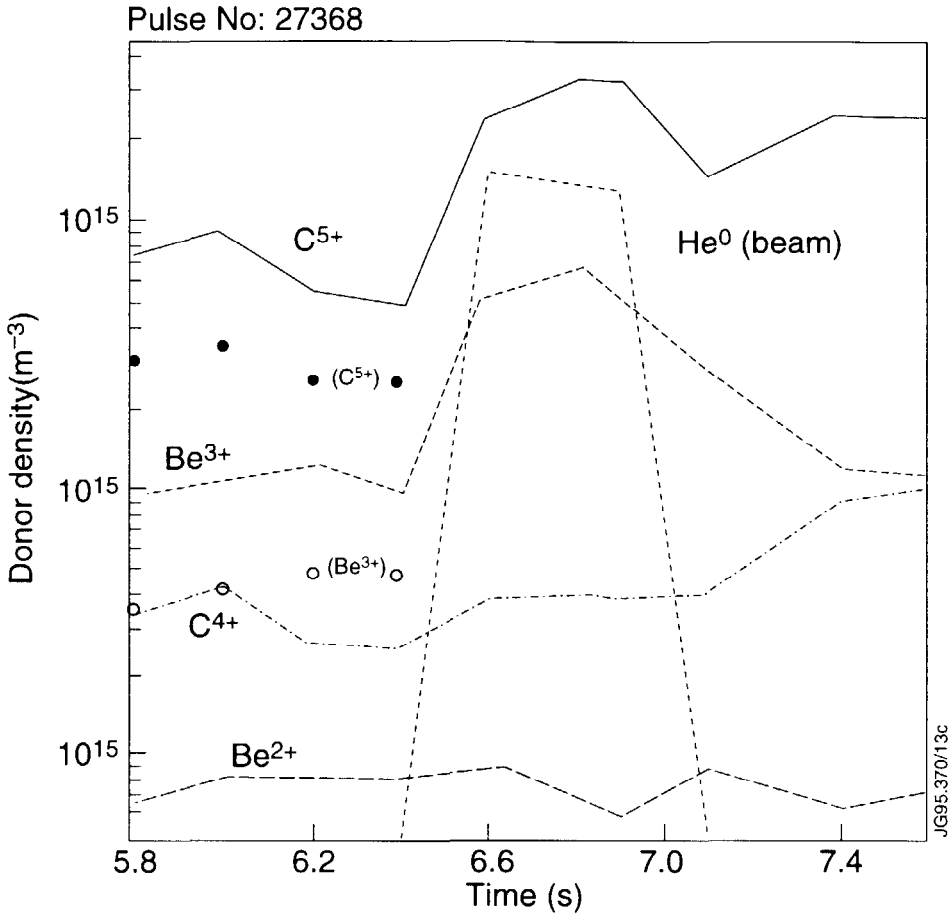


Fig.11: Evolution of model calculated densities of [H] and [He] ions of impurities, and of beam injected helium atoms in the plasma core. Densities of $Be^{3+}$, $Be^{2+}$, $C^{5+}$, and $C^{4+}$ ions are shown. Up to 6.4s these evolve under the influence of recycled thermal deuterium atoms and ≅1.6MW of 130kV deuterium atoms injected at oct.8. At 6.4s ≅6MW of 120kV $^4$He atoms are injected at oct.4. The solid(•) and open(o) circles show respectively the modeled density of $C^{5+}$ and $Be^{3+}$ if the oct.8 NBI were not present.

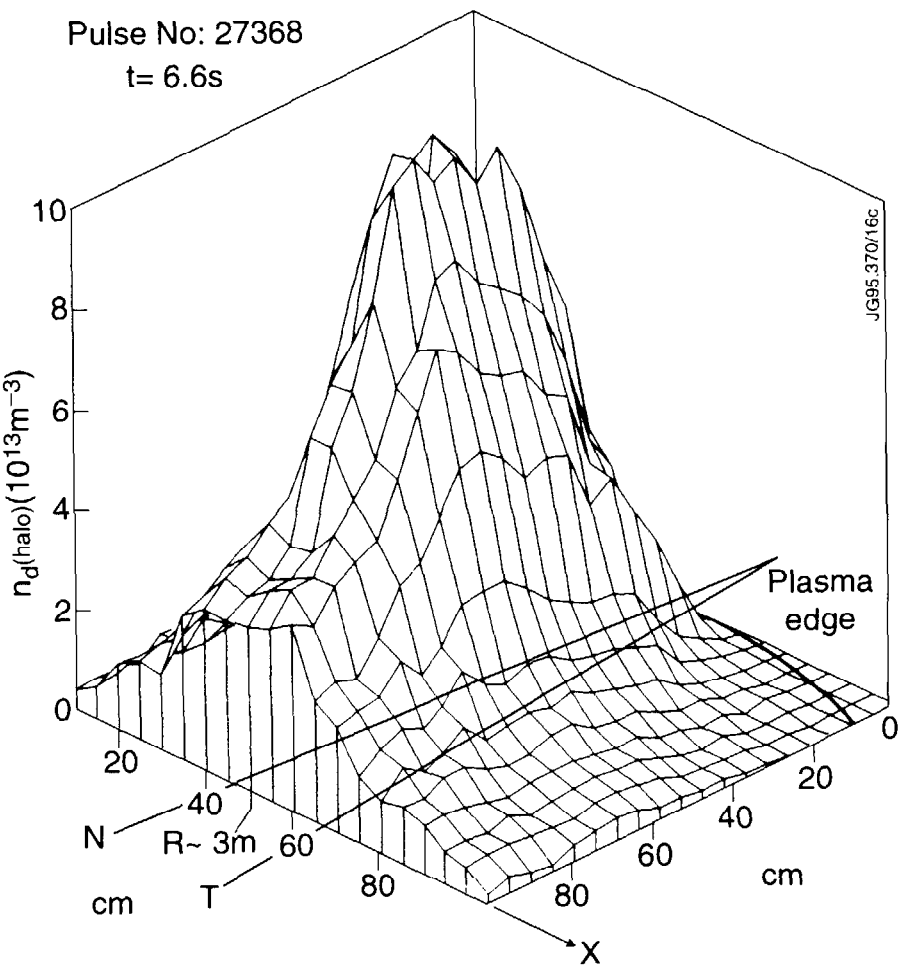


Fig.12: Spatial distribution of halo atoms in the horizontal mid-plane of the torus for pulse #27368 at t = 6.6s. The coordinate X≅50cm of the first cross-section corresponds to the geometric center of the plasma. Directions of the "normal"(N) and "tangential"(T) beams are shown.

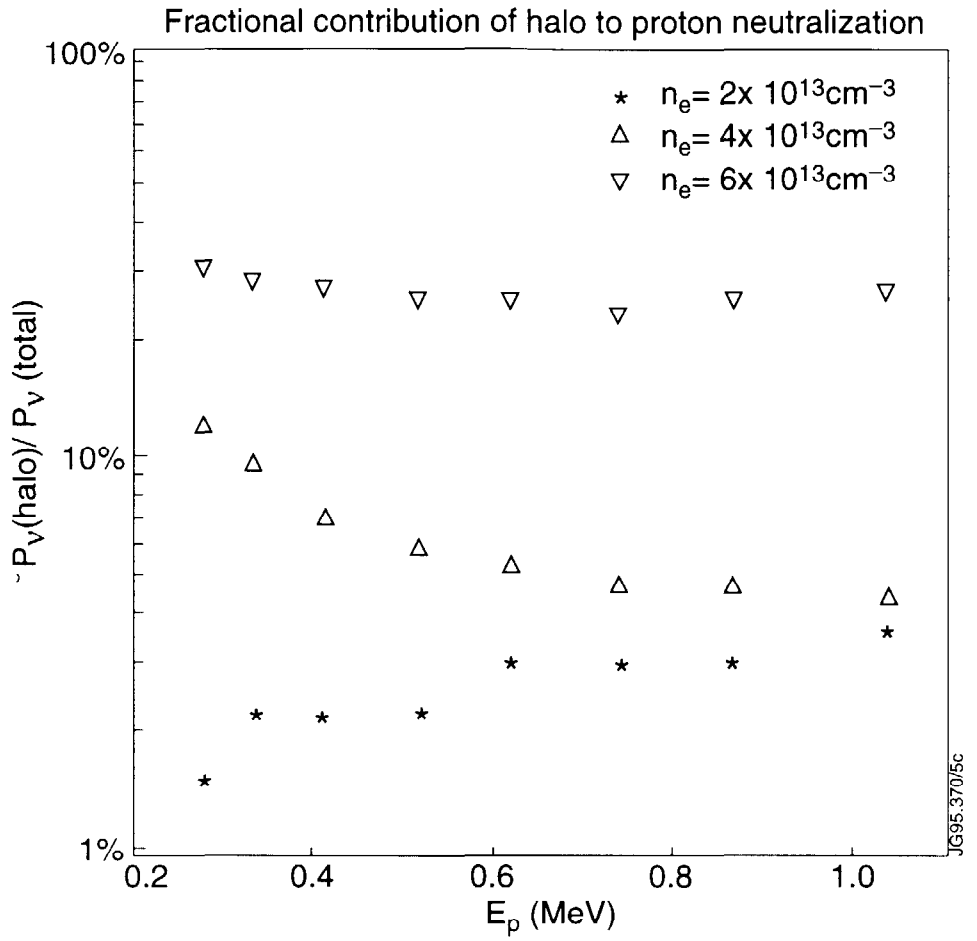


Fig.13: Variation with proton energy of fractional contribution of halo atoms to total neutralization rate for protons, for different values of plasma electron density $n_e$. The figure shows that as a function of energy the halo contribution is nearly constant for $E_P \geq 0.4$ MeV. As function of $n_e$ the halo contribution becomes significent, exceeding 5%, only when $n_e > 4x10^{19}\ m^{-3}$ .

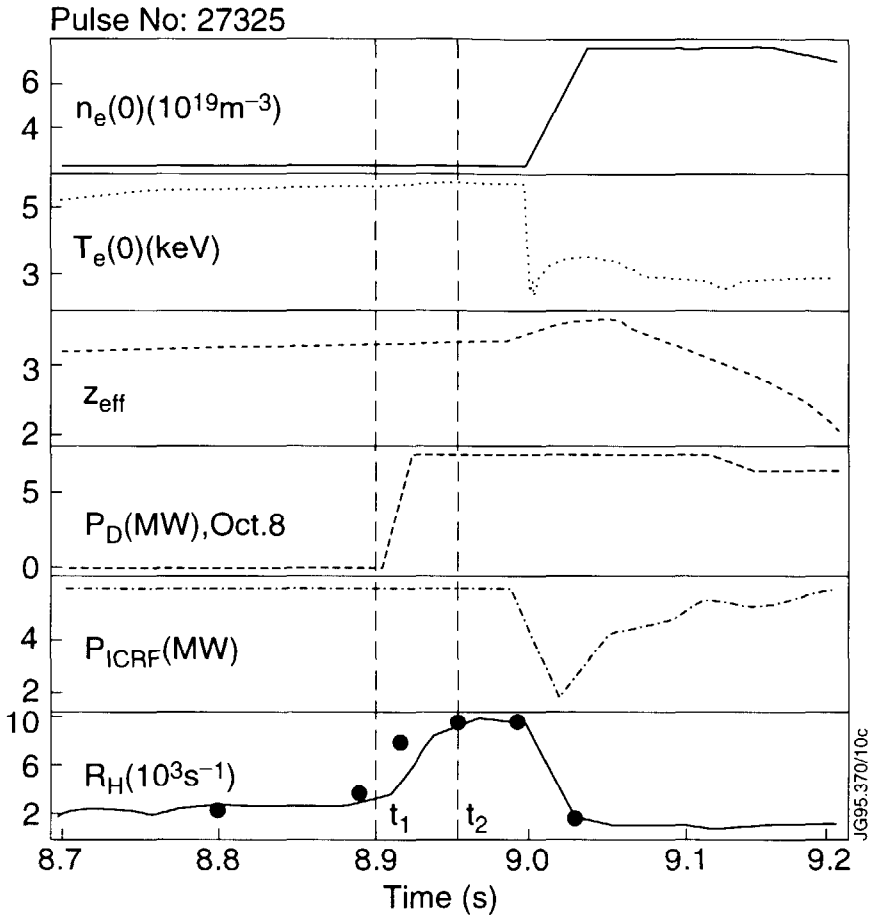


Fig.14: Evolution of plasma parameters, ICRF and NBI heating powers and NPA count rate for channel #1. Note that soon after t1 the flux of hydrogen to the NPA increases due to NBI at oct.8, toroidally ≅10m away from the NPA in oct.4. Background thermal deuterium density $n_d$ may be deduced by matching $\bar{f}(E_P)$ at two close time points t1 and t2 on either side of a controlled change in total deuterium atom density effected by NBI. Modeled evolution of $H^0$ count rate is shown as solid points, using the best value of $n_d$ .

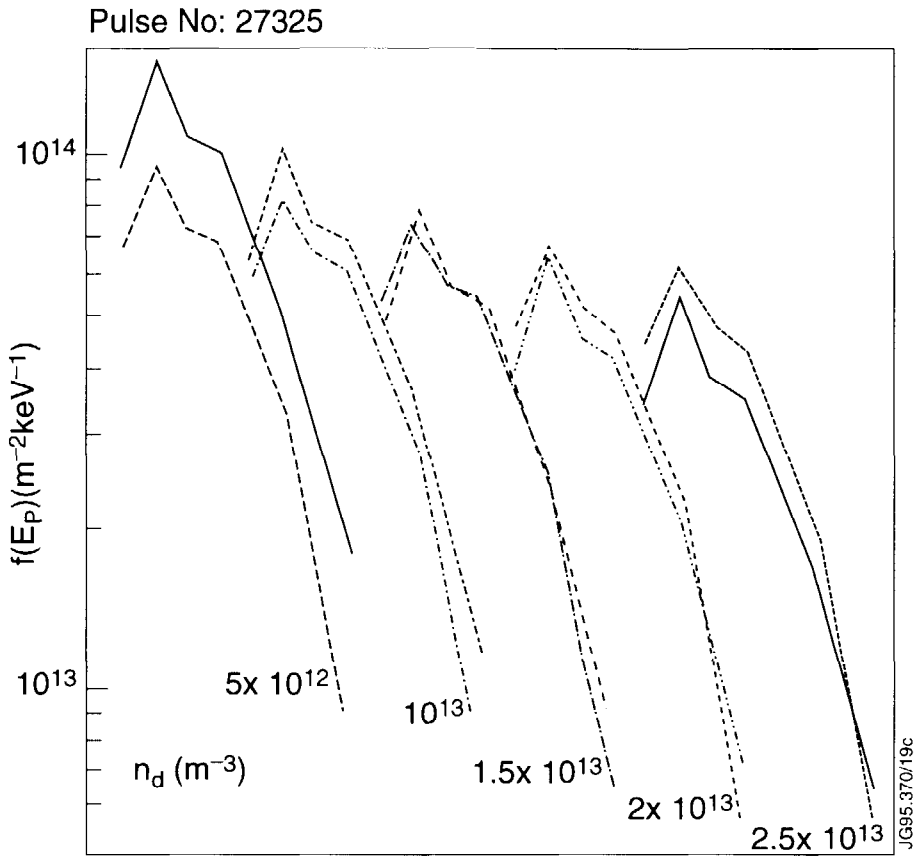


Fig.15: Proton energy distribution function $\bar{f}(E_P)$ inferred at time points t1 and t2 in pulse #27325 in fig.14. Background thermal deuterium atom density $n_d$ was iterated to obtain agreement between $\bar{f}(E_P)$ at t1 and t2. Impurity confinement time was assumed to be constant at $\bar{\tau}_Z = 1$ s. Best match was obtained with $n_d = 1.5 \times 10^{13}$ $m^{-3}$ .

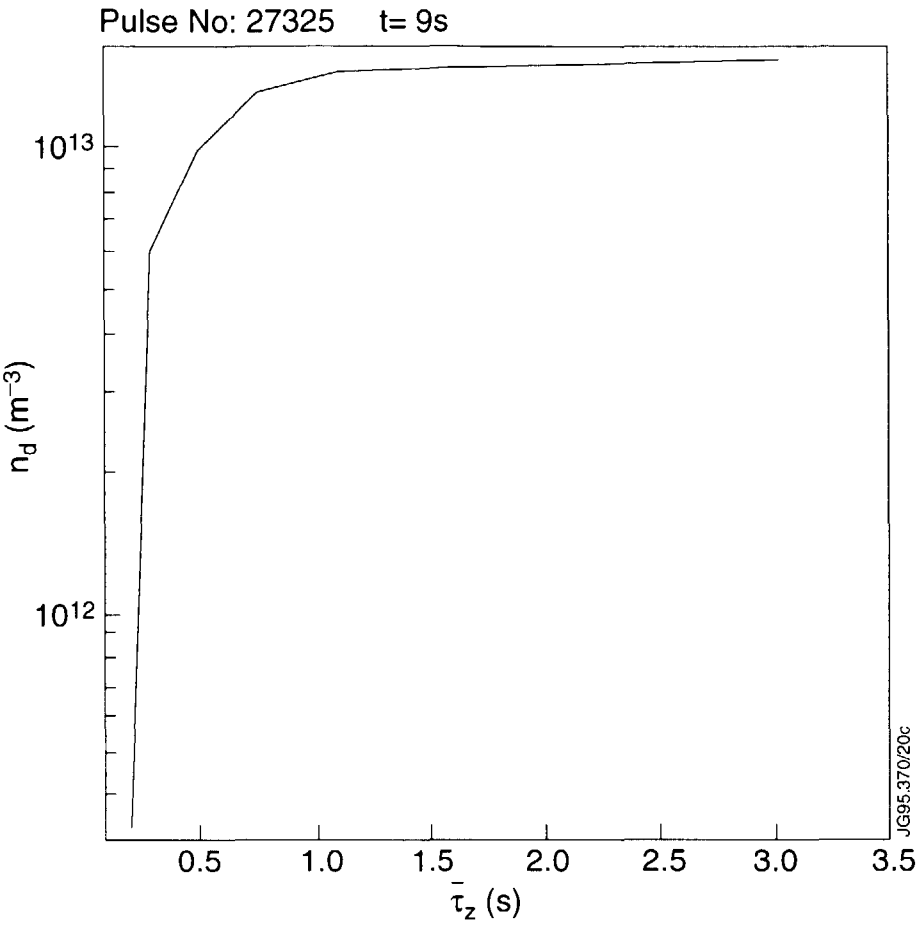


Fig.16: Sensitivity of inferred $n_d$ to assumptions about the magnitude of impurity ion confinement time $\bar{\tau}_Z$ in pulse #27325 at time t1. We see that for $\bar{\tau}_Z > 0.5$s the inferred $n_d$ is accurate to within ±25%.

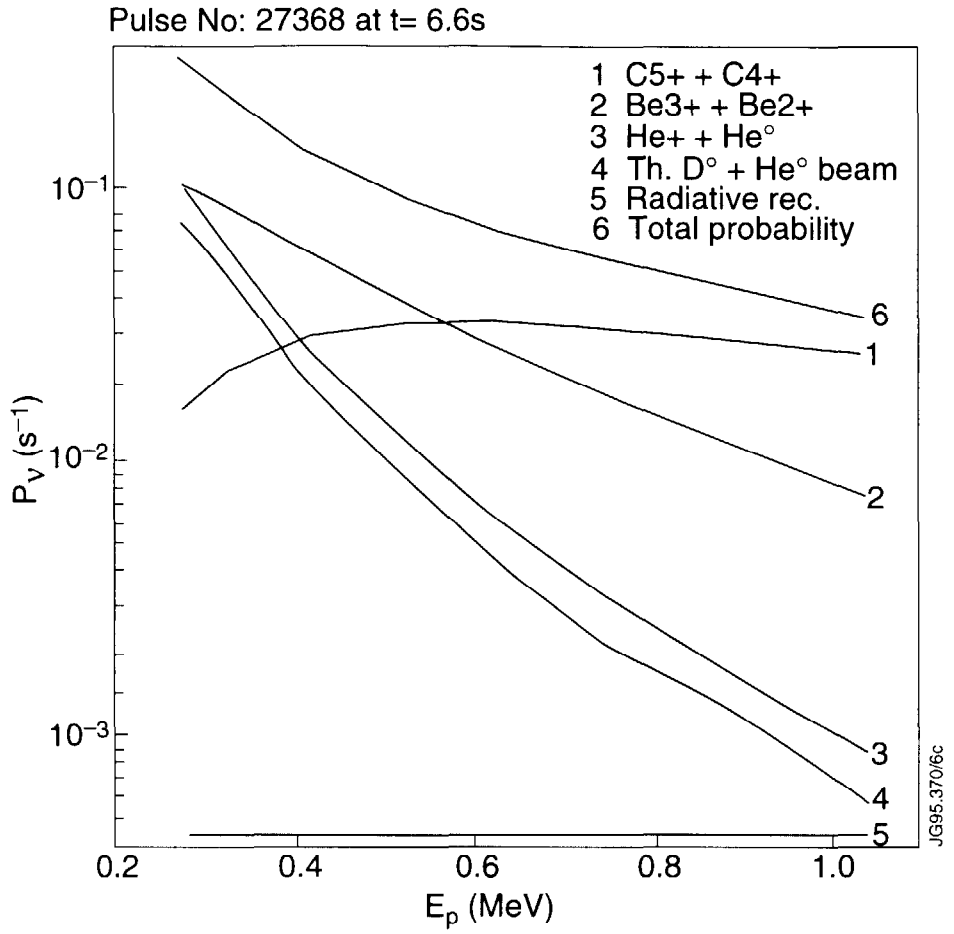


Fig.17: Contribution to total proton neutralization probability in pulse #27368 at 6.6s due to different charge donors. (#1) due to $C^{5+}$ and $C^{4+}$ ions, (#2) due to $Be^{3+}$ and $Be^{2+}$ ions, (#3) due $He^{+}$ ions and thermal He atoms, (#4) due to ≅ 5.8 MW of 120kV He beam atoms from oct.4 and thermal D atoms, (#5) due to radiative recombination, (#6) sum of all above contributions to give total neutralization probability $P_V$ ($E_P$).

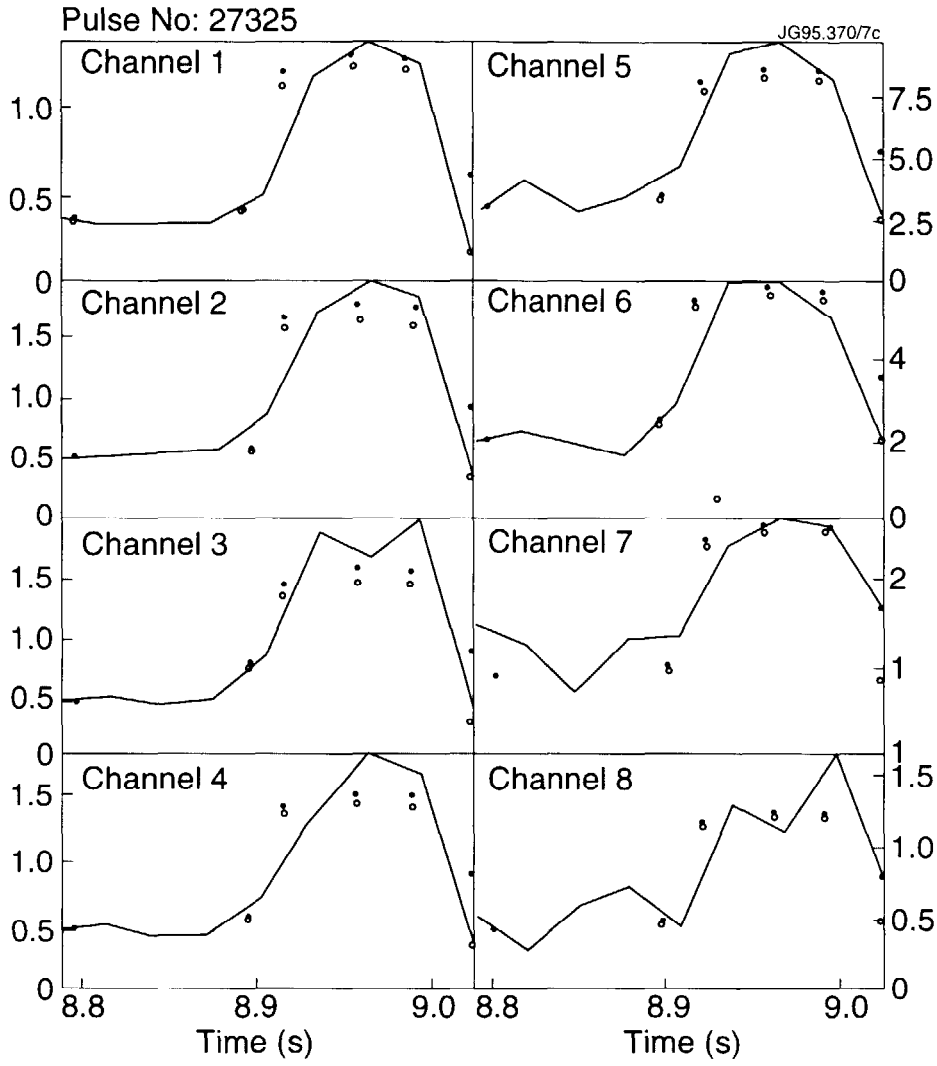


Fig.18: Modeling of evolution of hydrogen flux in pulse #27325. Figure shows that flux at all energies can be modeled simultaneously. The solid points (•) show the modeled flux without taking into account changes in attenuation during the pulse, whereas the open points (o) show the calculated flux taking into account evolving attenuation of beam and exiting hydrogen atoms. The latter underlines the need to properly treat evolution of plasma transparancy.

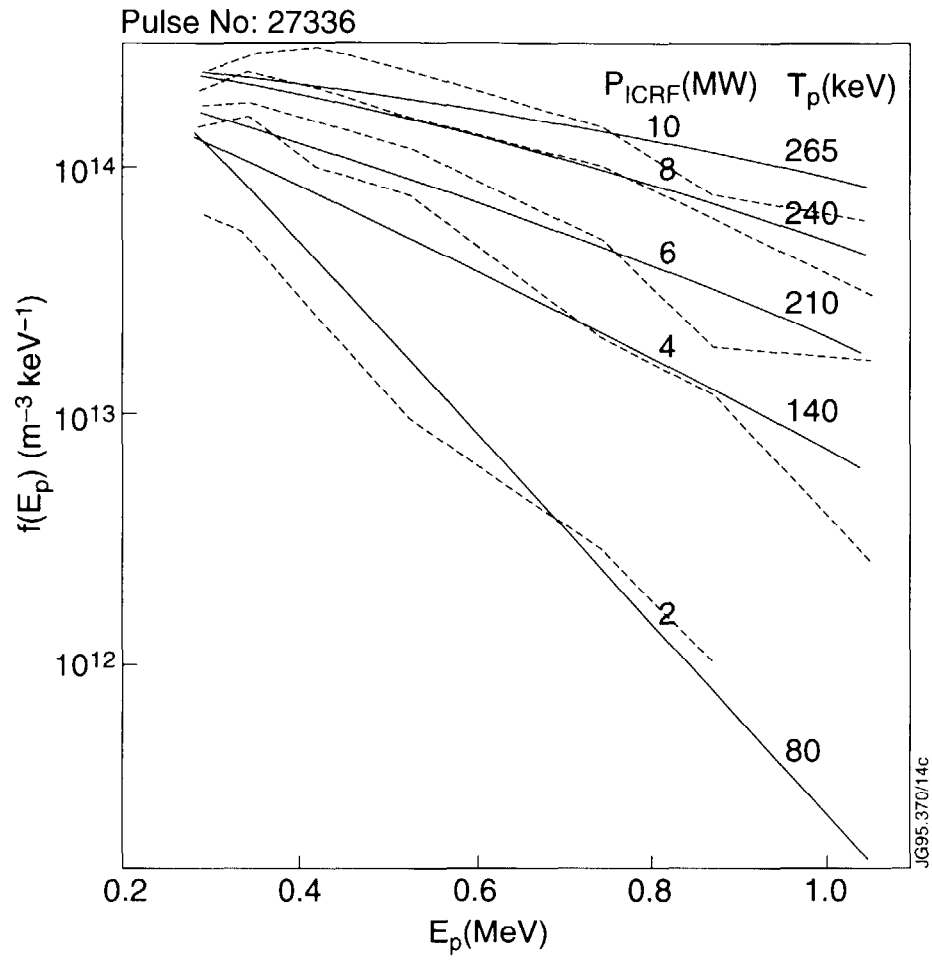


Fig.19: Best fitting Stix-like proton energy distribution function for pulse #27336, showing its variation with applied ICRF power. The best fit is to measured energy distribution function $\bar{f}(E_P)$(dashed curves) which was inferred from the measured hydrogen flux. We see that the conjecture of saturation of proton tail temperature with increasing ICRF power in[33] can not be sustained.

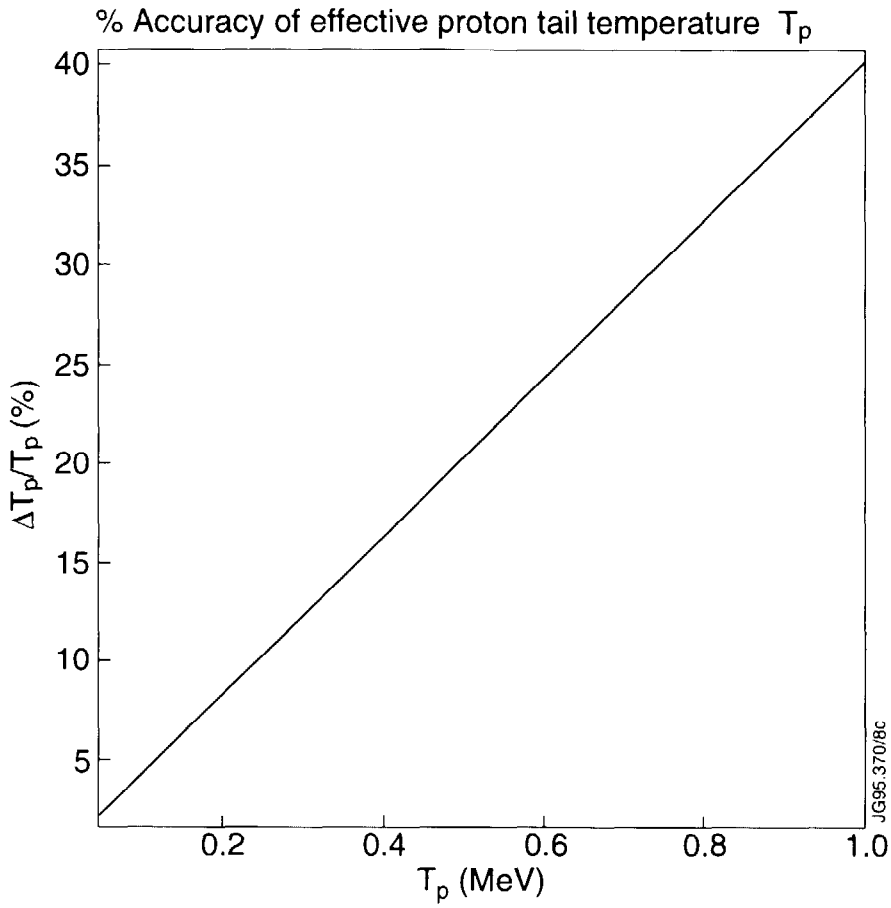


Fig.20: Accuracy $\Delta T_P / T_P$ of tail temperature $T_P$ associated with the energy distribution function of ICRF driven protons, in the energy range $E_P > 0.6$ MeV versus $T_P$ .

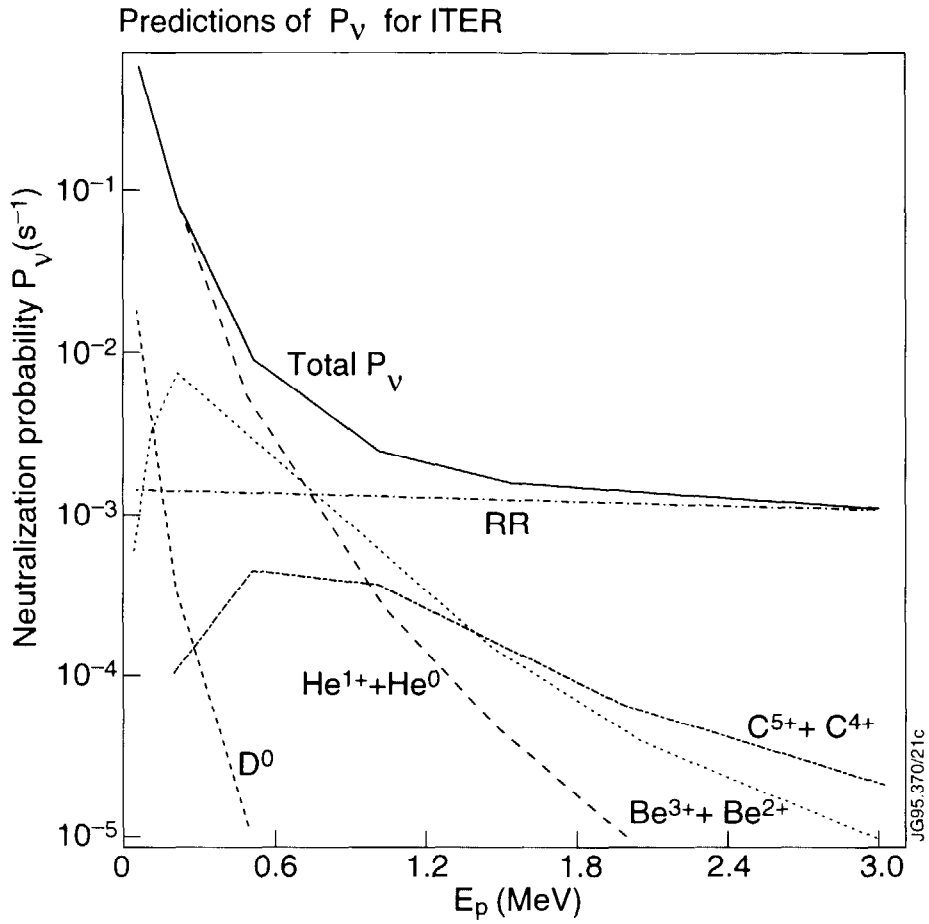


Fig.21a:Proton neutralization probability $P_\nu$ at the center of plasma in ITER as a function of $E_p$ due to different impurity donor ions with $\tau_Z$ = 2.5s, assuming forecast impurity levels in ITER plasmas, given as 20% He, 1% Be and 0.1% C.

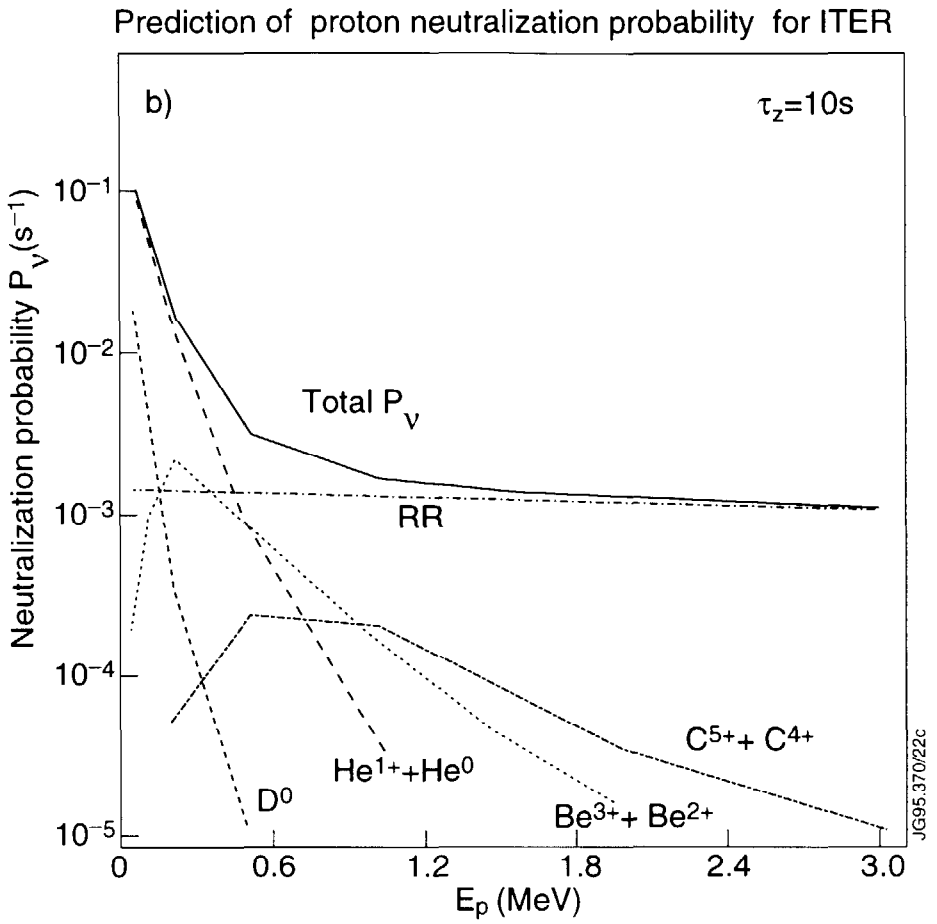


Fig.21b:Proton neutralization probability $P_\nu$ at the center of plasma in ITER as a function of $E_P$ due to different impurity donor ions with $\tau_Z$ = 10s, assuming forecast impurity levels in ITER plasmas, given as 20% He, 1% Be and 0.1% C.